cancers

MDPI

Article

Controlled Intra-Tumoral Delivery of Doxorubicin from a Ceramic Biomaterial Combined with Systemic Chemotherapy for Treatment of an Aggressive Osteosarcoma in Mice

Tova Corbascio [1,*], Hadis Alidadi [1], Jintian Huang [1], Tova Alm [1], Vėtra Markevičiūtė [2], Jacob Engellau [3,4], Lars Lidgren [1], Mathias Lidgren [1], Magnus Tägil [1] and Deepak Bushan Raina [1]

[1] Department of Clinical Sciences Lund, Orthopedics, Lund University, 221 84 Lund, Sweden; hadis.alidadi@med.lu.se (H.A.); jintian.huang@med.lu.se (J.H.); lars.lidgren@med.lu.se (L.L.); mathias.lidgren@med.lu.se (M.L.); magnus.tagil@med.lu.se (M.T.); deepak.raina@med.lu.se (D.B.R.)
[2] Department of Orthopedics and Traumatology, Lithuanian University of Health, Sciences, 50009 Kaunas, Lithuania; vetramarkeviciute@gmail.com
[3] Department of Clinical Sciences Lund, Medical Radiation Physics, Lund University, 221 84 Lund, Sweden; jacob.engellau@med.lu.se
[4] Department of Hematology, Oncology and Radiation Physics, Skåne University Hospital, 221 85 Lund, Sweden
* Correspondence: to5146co@lu.se; Tel.: +46-761-64-69-88

Simple Summary

Osteosarcoma treatment comprises chemotherapy and surgery, with doxorubicin (DOX) being a cornerstone among the three chemotherapeutic drugs commonly used for treatment. The aim of this research was to explore whether intratumoral delivery of DOX in conjunction with the standard-of-care systemic chemotherapy protocol could be tolerated and further improve the treatment response in an experimental osteosarcoma model in mice. The results of this research show that local delivery of DOX, achieved using a ceramic drug delivery system, led to an increased local treatment response when compared with systemically administered DOX. It is also demonstrated that the addition of local DOX combined with systemic chemotherapy was well-tolerated and had improved tumor-impeding effects with respect to the current chemotherapy protocol. The results of this study open up a potentially new treatment option for poor responders with this fatal disease.

Abstract

Background/Aim: Osteosarcoma (OS) treatment consists of chemotherapy with methotrexate, adriamycin (doxorubicin) and platinol (MAP) combined with intercalated surgery, resulting in a 5-year survival rate of 50–60%. We recently demonstrated that local delivery of doxorubicin via a microparticulate hydroxyapatite-based biomaterial (DASH) could efficiently impede tumor growth in subcutaneous OS; however, its effect in an orthotopic intraosseous OS remains unknown, particularly in conjunction with systemic MAP treatment. In this study, we performed two separate mouse model studies with the aim of (1) evaluating the effect of DASH in an orthotopic osteosarcoma model and (2) evaluating the efficacy and tolerability of DASH in conjunction with systemically administered MAP in a subcutaneous osteosarcoma model. Methods: In the first study, 56 mice were inoculated with human OS cells (i.e., h143B cells) in the proximal tibia. After 10 days, the mice were divided into seven treatment groups, of which group G2 (systemic DOX) was compared with groups G5–G7, which were treated with increasing doses of DOX delivered via DASH. The tumor-impeding response was evaluated via micro-CT (day 14), PET-CT (day 21) and tumor measurements (post-mortem). In the second study, 45 mice were inoculated subcutaneously with 143B cells and, 10 days later, groups G2–G5 were treated locally with increasing DASH doses, followed by two cycles of systemic MAP for all groups. On day

Check for updates

Received: 24 September 2026
Revised: 21 October 2026
Accepted: 2 November 2026
Published: 12 November 2026

Copyright: © 2026 by the authors. Licensee MDPI, Basel, Switzerland. This article is an open access article distributed under the terms and conditions of the Creative Commons Attribution (CC BY) license.

31, the animals underwent PET-CT examination followed by euthanasia and tumor measurements. Results: In both experiments, DASH treatment resulted in significantly lower tumor activity, tumor volume and weight. Micro-CT examination in the orthotopic model demonstrated that DASH treatment protected the bone from osteolysis. The subcutaneous study revealed that the mice were able to tolerate DASH, even in conjunction with systemically administered MAP. Conclusions: Intratumoral administration of DASH impeded OS growth in both animal models and protected bone against tumor-induced osteolysis. Furthermore, DASH was well-tolerated when administered in conjunction with systemic MAP therapy, indicating its potential therapeutic neo-adjuvant value in poor responders.

Keywords: osteosarcoma; biomaterials; local treatment; doxorubicin

1. Introduction

Osteosarcoma (OS) is the most common primary bone malignancy, with an incidence of one to three per million people worldwide [1]. These tumors occur mainly in the growth plate of long bones such as the femur, humerus and tibia. The incidence has a bimodal age distribution with most occurrences being in adolescent years and a second spike occurring in the elderly, after 60 years of age [2]. In such cases, the disease is often secondary to Paget's disease and arises in the axial skeleton [3,4]. Metastatic disease is detected in 18% of patients upon diagnosis, most commonly occurring in the lungs [5]. The standard treatment regimen for OS comprises neoadjuvant chemotherapy with intercalated surgery, followed by adjuvant chemotherapy [6]. As cytostatic agents, a combination of the three drugs, namely, methotrexate, doxorubicin and cisplatin, is used [6]. The multidrug treatment regimen comprises two neoadjuvant cycles followed by surgery, followed by four adjuvant cycles, collectively referred to as the MAP protocol.

After the inception of the MAP protocol, the OS survival rate increased from 20% to 60% during the 1970s and 1980s, without any further improvement since then [7]. The European and American Osteosarcoma Study (EURAMOS-1) included 2260 patients with high-grade resectable localized or metastatic OS treated with the MAP protocol. Its results indicated a 5-year event-free survival (EFS) of 54%, and the 5-year overall survival was calculated to be 71%; furthermore, localized disease had a 5-year EFS of 60% and an overall 5-year survival of 76% [8]. Even though implementation of the MAP protocol resulted in a significant increase in survival rates, metastatic and recurrent disease is still associated with poor survival rates, with the five-year survival rate being less than 25% [7,9]. The recurrence rate is still 30–40% in patients initially diagnosed with local and non-metastatic disease despite extensive chemotherapy and radical surgery [8,10,11], and poor response to neoadjuvant treatment is not uncommon [12,13]. Approximately 50% of patients treated with neoadjuvant chemotherapy are classified as poor responders, i.e. patients who show <90% of necrosis within the tumor tissue on biopsy after the end of two neoadjuvant MAP cycles [12].

The oncogenic driving factors for the development and spread of osteosarcoma have been difficult to establish, and a multitude of different mutations and duplications are responsible for the complexity of the somatic genome of osteosarcoma [14]. The complex genomic landscape of OS combined with significant cellular heterogeneity has hindered the development of molecular targeting treatments and immunotherapy [1], which, in turn, has led to stagnation of the development of treatments other than chemotherapy and the MAP protocol [15].

One of the intrinsic challenges imposed by current systemic drug delivery methods is their non-specificity regarding the intended target tissue. In research on drug targeting and

passive nanoparticle distribution, it has been shown that over 95% of all administered drugs passively accumulate in other organs and sites not intended for treatment [16]. Not only could this be the cause of the poor response to treatment, but it may also lead to adverse reactions which can be incredibly detrimental for patients, thus reducing their quality of life and resulting in a need to reduce the dose or delay treatments [17,18]. In this regard, the side effects associated with treatment with doxorubicin (an anthracycline)—including myelosuppression and cardiotoxicity—are dose-limiting [19].

Radical surgery, as a treatment for osteosarcoma or bone metastasis of other cancers, is often combined with reconstructive surgery and implantation of different supporting materials for pain relief and mechanical stability [18]. One such material is a mixture of hydroxyapatite (HA) and calcium sulfate (CaS). HA is the inorganic component of our skeleton, while CaS (also known as plaster of Paris) binds the HA particles together. Post-mixing, the CaS/HA material is an injectable and moldable paste, which is often used after bone debridement or resection to fill bone voids [18]. The material has a non-exothermic setting reaction, meaning that it can set at body temperature (unlike other utilized bone cements) [20,21]. It can also be effectively loaded with a wide range of drugs, allowing for local targeting of bone disease, due to its non-exothermic setting reaction [22,23]. The proposed advantages of drug delivery using CaS/HA are locally sustained and prolonged exposure, with a controllable and minimized initial burst release. This local delivery approach also ensures reduced exposure in tissues that are not the intended target for treatment [18,24].

In a local drug delivery system, drug release is determined by the material's structure, physio-chemical properties, the interactions between carrier material and drug, and the drug loading strategy (e.g., mixing the drug with the wet or dry component of the material) [25–27]. When incorporated into a biodegradable material, the material degradation kinetics impact the drug release mechanisms [26,27]; such mechanisms include material degradation itself, as well as breakage of chemical bonds, diffusion and absorption–desorption [26,27]. Due to CaS/HA cement having a slower degradation rate than the drug release rate, the release of the drug is considered to depend on either diffusion or physio-chemical interactions between the drug and the material, both of which can be controlled to achieve optimal drug release.

As DOX is the cornerstone drug in the MAP protocol, our group has previously investigated local DOX delivery via the CaS/HA delivery system. In an earlier study performed by Yang et al., DOX was shown to electrostatically interact with hydroxyapatite (HA) [28]. HA is a naturally occurring calcium phosphate found in the skeleton [29] and has two binding sites with an affinity for macromolecules, with one being the C-site containing Ca- ions and the second being the P-site containing phosphate groups [30]. In turn, doxorubicin has multiple hydroxyl groups to which the C- and P-sites can form weak electrostatic bonds [31]. In our previous study, we found that DOX bound to HA was endocytosed and delivered to the lysosomes, the low pH conditions of which reversed the electrostatic interactions between HA and DOX, thus freeing the DOX [28]. Most of the DOX then accumulated in the mitochondria, thereby inducing mitochondrial damage and cell death [28]. Previous studies have shown that the tumor microenvironment is characterized by a pH range of 5.5–6.8, thus increasing the opportunity to free the DOX in close proximity to the chosen treatment site [32].

Local drug delivery using doxorubicin is not entirely novel, as it is presently performed clinically; however, this use is not routine. One example of local DOX delivery is in transarterial chemoembolization (TACE), used as a standard of care for early- and intermediate-stage hepatocellular carcinoma [33]. Multiple studies have also evaluated doxorubicin as a local treatment for bladder cancer with intravesical instillation, for treatment of papillary carci-

noma and in situ carcinoma [34]. Even though local chemotherapy treatment potentially offers advantages such as a higher intratumoral drug concentration, expanded treatment options for inoperable patients and reductions in systemic doses, which otherwise carry sequential adverse reactions, clinical adaptations remain underdeveloped at present.

This situation might be explained by the difficulty of developing a platform with the ability to maintain high and prolonged concentrations which can be instilled in solid tumors such as carcinomas and sarcomas. Therefore, this study investigates two different pertinent questions related to the local delivery of DOX within a solid tumor using a CaS/HA drug delivery system. The purpose of the first study was to investigate the efficacy of a local DOX delivery system using a CaS/HA biomaterial (DASH) compared with systemic doxorubicin treatment, in mice inoculated with highly aggressive OS cells in the proximal tibia. The aim of the second study was to evaluate the efficacy and tolerability of DASH as an add-on to standard MAP treatment, compared with standalone MAP, in a mouse model of human osteosarcoma. We hypothesize that a high local dose of DOX delivered intratumorally could efficiently hinder the growth of aggressive OS.

2. Materials and Methods

2.1. Materials

The nude athymic mice (Fox1$^{nu/nu}$) were purchased from Janvier Labs, Le Genest-Saint-Isle, France. Doxorubicin hydrochloride powder was kindly provided by Teva Pharmaceuticals, Amsterdam, Europe. The CaS/HA carrier material was kindly provided by Lithea AB (Lund, Sweden), which was provided in powder form after gamma sterilization. Human osteosarcoma cells (h143B) were purchased from ATCC, CRL-8303, (Manassas, VA, USA) and RPMI medium and heat-inactivated fetal bovine serum were bought from Life Technologies, Bleiswijk, The Netherlands. MTT reagent was purchased from Sigma Aldrich, St. Louis, MO, USA. The type I collagen scaffold used as a tumor-seeding material was purchased as part of the InductOS bone graft kit from Medtronic, Minneapolis, MN, USA. Commercially available doxorubicin (Teva Pharmaceuticals, 2 mg/mL), methotrexate (Ebewe, Unterach am Attersee, Austria, 2 mg/mL) and cisplatin (Ebewe, 1 mg/mL) were purchased from a local pharmacy (Apoteket AB, Solna, Sweden) for intravenous administration in animals receiving systemic MAP treatment.

2.2. Study Design

2.2.1. Study 1: Orthotopic Tumor Comparing DASH to Systemically Administered DOX

A total of 56 mice were inoculated with h143B cells in the proximal tibia (for a timeline of the study, see Figure 1). The mice underwent treatment on day 10 post-inoculation. To recreate a clinical scenario of neoadjuvant treatment and reduction in tumor mass in preparation for radical surgery, their tumors were either (1) left untreated (control group) or (2) exposed to systemic administration of doxorubicin (systemic treatment), (3) treated with a local injection of carrier-free doxorubicin inside the tumor, (4) treated with a ceramic material without a cytostatic agent (biomaterial control group) or (5–7) treated with a combination of a ceramic material and doxorubicin at three different concentrations (doxorubicin-loaded biomaterial). A detailed description of all the treatment groups is provided below. To track tumor development and the treatment effects, all mice underwent micro-CT at 14 days and PET-CT at 21 days post-intervention. Thereafter, the experiment reached its endpoint, the mice were euthanized, and the volume and weight of their tumors were quantified. After euthanization, the legs and vital organs were harvested for histology.

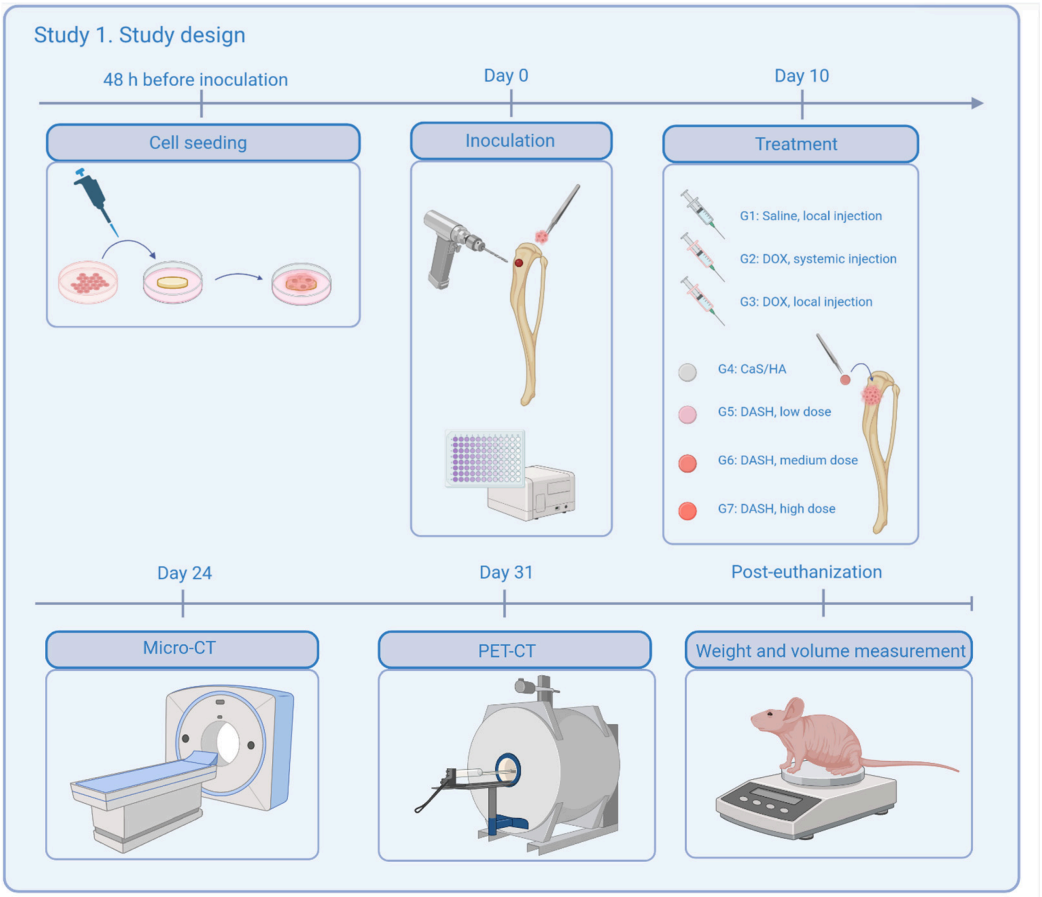


Figure 1. Timeline and study design for the orthotopic tumor model. On day 0, the mice were inoculated with h143B cells seeded on a collagen scaffold. Ten days after inoculation, the animals were examined for tumors and treatment was initiated. On day 14 after treatment administration (24 days after tumor inoculation), the animals underwent micro-CT imaging. On day 31 after tumor inoculation, PET-CT imaging was performed on all animals. After imaging, the animals were euthanized and the volume and weight of the tumors were quantified. Histology was also performed after measurements. Image created using BioRender.com.

2.2.2. Study 2: Subcutaneous Tumor Model Evaluating DASH in Conjunction with MAP: Evaluation of Efficacy and Tolerability

Another study was conducted in immunocompromised mice. A total of 45 mice were inoculated with 143b cells in subcutaneous tissue. Afterwards, they were divided into five treatment groups, differing in local treatment and treatment was initiated on day 11. Group 1 was left without local treatment while groups 2–5 underwent local treatment. All animals were subjected to the MAP regime, and doxorubicin, cisplatin and methotrexate were given in two cycles (Figure 2). Doxorubicin and cisplatin were administered on days 13 and 22 after tumor cell inoculation, while methotrexate was given on days 16 and 25 after tumor inoculation. Group 1 received the standard of care treatment (i.e., the MAP regime only). Group 2 was implanted with a CaS/HA-pellet. Group 3–5 were implanted with a CaS/HA-pellet loaded with doxorubicin (DASH) at three different doses; Groups 3, 4 and 5 were administered a low dose, intermediate dose and high dose, respectively. The primary outcome was tumor metabolic activity calculated using PET-CT on day 31, as the terminal treatment effect outcome. Secondary outcomes were tumor weight and volume, calculated using an analytical scale and vernier calipers for measurements performed post-

euthanization and once a week during the treatment period. Histology was also carried out for qualitative screening of active tumor areas.

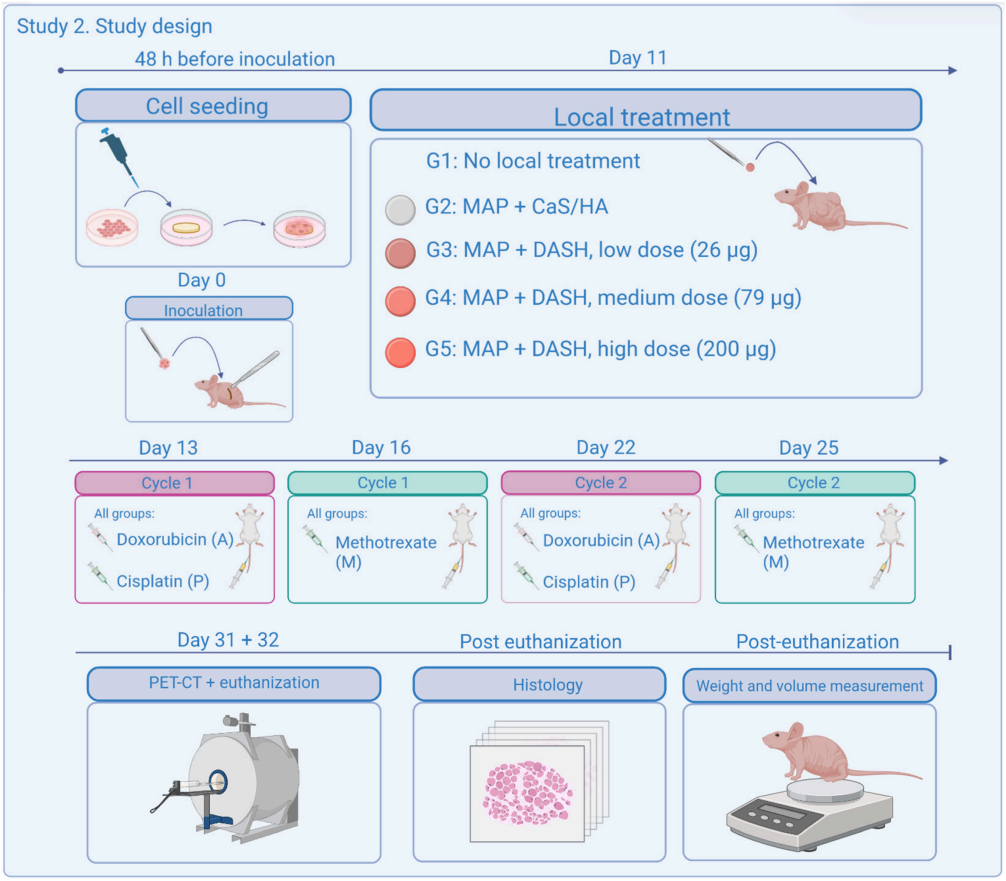


Figure 2. Experimental timeline of study 2. h143b cells were seeded on a collagen scaffold and inoculated into the subcutaneous tissue in 45 nude mice. On day 11, the animals were divided into five treatment groups, of which Groups 2–5 underwent local treatment while G1 served as a control group, which received no local treatment. G2 was treated with excipient (CaS/HA-pellet), G3 was treated with low-dose DASH (26 µg) and G4 and G5 were treated with medium-dose (79 µg) and high-dose DASH (200 µg). Thereafter, all groups received two cycles of the MAP protocol; doxorubicin and cisplatin were administered intravenously on days 13 and 22, while methotrexate was administered on days 16 and 25. PET-CT was performed on day 31 or 32 to measure tumor activity. As secondary outcome measurements, histology, weight and volume assessments were performed after euthanization. Image was created in BioRender.com.

2.3. Study Methods—Study 1: Orthotopic Osteosarcoma Model—Investigating Treatment Effect of DASH Compared with Systemic DOX Administration

2.3.1. Cell Culture and Creation of Cell Suspension

The cell line used for tumor inoculation was the human osteosarcoma cell line 143b. The cells were cultured using a complete medium consisting of RPMI 1640 with FBS (10 vol%), penicillin (1 vol%) and streptomycin (1 vol%) in T75-flasks. At 80% confluency, the cultivation was concluded and the cells were harvested using EDTA-Trypsin and diluted in medium (2:1 trypsin). The cells were then centrifuged and counted using a Bürker chamber (Medtronic, Minneapolis, MN, USA). The cells were diluted to a concentration of 2×10^5 cells per 2.5 µL.

2.3.2. Seeding the Scaffold

The type I collagen scaffold, sold as part of the InductOS bone graft kit (Medtronic, Minneapolis, MN, USA), was cut into a cylindrical shape using a 2 mm biopsy punch. The scaffolds were disinfected by placing them in a falcon tube filled with 70% ethanol for 10 min, to stabilize the structure before washing it with phosphate-buffered saline (PBS). The ethanol was carefully removed using a pipette and PBS was added to the falcon tube. The tube was put on a shaker for 5 min and the PBS was removed. This step was repeated, with PBS added again; however, the tube was not put on a shaker. The contents of the tube were poured into a Petri dish, and the scaffolds were carefully collected using forceps and individually placed centered in a well of a 96-well plate. To each well, 200 µL of complete medium was added, followed by incubation of the plate at 37 °C for 1 hour.

Then, the medium was removed using a pipette and 2.5 µL of cell suspension (2×10^5 cells) was added onto the scaffold. The scaffolds were incubated for 30 min to ensure the cells had time to settle on the scaffold surface, before adding an additional 2.5 µL of complete medium to the well. After another hour of incubation, 200 µL of medium was added, and each well was observed under a microscope to ensure that no significant cell leakage could be observed. At 48 h after seeding, the scaffolds were implanted into the mice. Cell seeding was performed on 3 separate days, following the same experimental procedure at each time point.

2.3.3. Tumor Inoculation

To establish the xenograft human osteosarcoma model in Fox1 nude mice, 4–5-week-old female athymic nude $Fox1^{nu/nu}$ mice were procured from Janvier Labs, France. The mice were anesthetized via isoflurane (2–3%) sedation, in a 1:1 mix of oxygen and nitric oxide in an incubation chamber with a flow rate of 0.2 L/min [28]. After disinfecting the skin with ethanol, a 2 mm skin incision was made over the proximal tibia and the area was cleared of covering tissue using a scalpel. Below the epiphysis (which could be located through visual inspection), a small hole was drilled using a handheld manual drill (diameter = 2 mm) until resistance from the posterior cortex was felt. Care was taken to not perforate the posterior cortex, as that would lead to cell leakage into the muscle. The cell-seeded collagen scaffold was then carefully inserted into the burr hole. The skin was closed with sutures. Cell viability evaluation at the end of each experimental day was performed on the cell-seeded scaffolds using MTT assay, as described elsewhere.

2.3.4. Preparation and Administration of Treatments

The mice were divided into the seven following treatment groups (with eight animals per group): local injection of saline (G1); systemic injection of DOX at a dose of 40 µg per animal (G2); local injection of carrier-free DOX at a dose of 40 µg per animal (G3); intra-tumoral implantation of a pellet consisting of a ceramic material (CaS/HA) (G4); and intra-tumoral implantation of a pellet consisting of a ceramic material (CaS/HA) loaded with DOX at a low dose (G5), an intermediate dose (G6) or a high dose (G7). All treatments were performed under isoflurane anesthesia. For each treatment group, two animal cages (with four animals in each) were chosen randomly. The animals were checked for visible tumors, and specimens with tumors that were difficult to see were noted in the surgical protocol.

For G1 mice, the skin was cut open over the tumor and 20 µL of NaCl 0.9% was administered into the tumor tissue using a 0.3 mL insulin syringe. The skin was closed with two stitches. The treatment was performed similarly in the G3 group, members of which received 20 µL of 2 mg/mL DOX solution for a total intratumoral DOX dose of 40 µg. G2 mice were treated with an injection of 20 µL of 2 mg/mL of DOX solution mixed

with 80 µL of NaCl 0.9% into the tail vein; the skin over the tumor was opened and the tumor was pricked using a thin needle to maintain similar tumor handling between all groups (Table 1).

Table 1. Experimental groups in the orthotopic OS study in nude mice. G1 mice were treated with an intratumoral injection of saline. G2 mice were treated systemically with an intravenous injection of doxorubicin (40 µg). G3 mice were treated with an intratumoral injection of doxorubicin (40 µg). G4 mice were treated with an intratumoral implantation of a pellet containing CaS/HA. G5, G6 and G7 mice were treated with an intratumoral implantation of a pellet containing CaS/HA loaded with doxorubicin at doses of 40, 150 and 300 µg, respectively.

Groups	Treatment	Administration Route	Dose DOX
G1	NaCl (0.9%) injection	Intratumoral	0 µg
G2	DOX injection	IV	40 µg
G3	DOX injection	Intratumoral	40 µg
G4	CaS/HA pellet	Intratumoral	0 µg
G5	CaS/HA pellet + low dose DOX	Intratumoral	40 µg
G6	CaS/HA pellet + medium dose DOX	Intratumoral	150 µg
G7	CaS/HA pellet + high dose DOX	Intratumoral	300 µg

Group G4–G7 mice were treated intratumorally with a ceramic material (CaS/HA), which was created by mixing powder and liquid components molded into 15 µL pellets. Each animal was treated with one pellet. The dry component for all groups comprised a mixture of calcium sulfate/hydroxyapatite (CSH 60 wt.%/HA 40 wt.%) with the addition of 3 wt.% calcium sulfate dihydrate (CSD) and 1.25 wt.% NaCl powder. For G4, the liquid component consisted of iohexol (240 mg/mL). For G5, 1.78 mg of DOX powder was first dissolved in 0.38 mL of iohexol (240 mg/mL), which was then mixed with 1 g of the CaS/HA powder to achieve a DASH pellet containing 40 µg DOX per pellet. In G6 and G7, 6.6 and 13.2 mg of DOX powder was dissolved in 0.38 mL iohexol (240 mg/mL), giving respective dosages of 150 µg (G6) and 300 µg (G7) per animal (Table 1).

One gram of the dry component was weighed in a 12-well plate and 0.38 mL of the liquid solution was added using a pipette. The components were mixed for 30 s before the paste was transferred to a silicone mold. To insert the drug-loaded pellet, the skin was incised and a small hole was created in the tumor using a needle. The pellet was then divided into smaller parts, which were all inserted into the medullary canal. Any remaining pellet that did not fit was placed immediately above the hole in the tibia. The skin was closed with two stitches, and the animals were monitored the following days to observe their sutures and tails.

2.3.5. Evaluation of Treatment Response: Primary Outcome Variables

Micro-CT

As 143B osteosarcoma cells are known to cause osteolysis of the bone, micro-CT was used as a tool to visualize the bone structure at a micro-structural level [35], enabling evaluation of the structural changes and bone destruction pattern after tumor inoculation. Micro-CT was performed on live mice under isoflurane anesthesia.

The settings of the scanner (Milabs U-CT micro-CT scanner) were as follows: X-ray voltage of 50 kV, X-ray current of 0.21 mA, exposure time of 0.75 s, an angle of 360 degree ultra scanning mode, angle step degree of 0.25, 1:1 binning and ultra-focus magnification.

CT was performed on day 14 after treatment to evaluate the bone structure in vivo. With the chosen settings, the pictures were reconstructed to a voxel size of 30 µm. Three-dimensional pictures were reconstructed using Seg32 (open source, University of Utah, Salt Lake City, UT, USA). For visualization of bone tissue, the threshold value was set

to 2300 Hounsfield Units for exclusion of tissue with lower density. The animals were then classified, according to the degree of bone destruction, as either no destruction (intact cortex, no signs of resorption), low cortical destruction (signs of resorption present and some remaining tissue in the metaphysis, but not a complete cortex) or high cortical destruction (the cortex destroyed in the metaphysis and the proximal tibial metaphysis were completely missing). The classification was performed by two observers, both of whom were not blinded to the treatment groups.

PET-CT

PET-CT was performed to visualize and quantify the metabolic activity of the tumor tissue at 21 days post-treatment [36] using a previously developed protocol [37]. Awake mice were administered ^{18}F-FDG (44.2 ± 7.3 MBq) intraperitoneally by diluting the radioactive tracer in NaCl solution. At 30 min post-injection, animals were anesthetized using isoflurane as previously described. Before the PET-scan, a CT-scan was performed 40 min post-injection to locate the skeletal source of the PET signal. At 61.4 ± 2.6 min, PET images were acquired using a small animal PET/CT-scanner (Mediso, Budapest, Hungary), except for the first scan which was performed at 91.5 ± 1.3 min. Four mice were scanned at a time, using a mouse bed that could accommodate four animals. Full-body high-resolution images were captured with a voxel size of 300 µm. Reconstruction of PET images was performed using the Tera-Tomo™ three-dimensional (3D) PET image reconstruction engine (Nucline NanoScan 3.05.027, Mediso, Hungary). The CT images acquired prior to each PET scan were used as an anatomical reference and for attenuation correction. The total injected activity, tracer decay before scan start and region of interest were documented to calculate the PET-CT-based tracer uptake. Once all PET-CT reconstructions were deemed sufficient, animals were sacrificed by performing cervical dislocation. The PET-CT-based tumor response was quantified according to the 18 F-FDG uptake in the tumor. A region of interest was placed over the active area to calculate tumor volume and activity. PET-CT data are presented as the percentage of total radioactivity measured in the tumor (% injected activity in tumor), normalized radioactivity (i.e., % injected activity in tumor/tumor weight in grams) and tumor volume used for PET-CT quantifications.

2.3.6. Evaluation of Treatment Response: Secondary Outcome Variables

Volume and Weight

After euthanization, the tumors were measured using a vernier caliper and weighed. The two measurements of interest were the length and width of the palpable tumor. The volume of the tumor tissue was calculated using the following formula: Volume = Length * Width^2/2. The legs with the tumors were cut above the knee joint and weighed on an analytical scale.

Histology

Histology was performed for qualitative screening of active tumor areas. The legs were placed in formalin (4% v/v) for 24 h after harvesting to fix the tissue. The samples were then put in EDTA solution (10% w/v; pH 7.4; 4 degrees) for 4 weeks, for decalcification of the tissue. The solution was changed two times a week. Once the samples had decalcified, routine paraffin embedding was performed and the samples were cut to a thickness of 5 µm using a microtome. Slides were stained with H&E following routine histological procedures and digitized on an Olympus slide scanner.

2.4. Study Methods—Study 2: Subcutaneous Tumor Model Investigating Effects of Standard of Care: The MAP Regime and the Addition of DASH

2.4.1. Cell Seeding and Inoculation

For the second study, the cells used for tumor inoculation were the same as in study 1, and were cultivated using the same method and materials as described above. The cells were seeded on a type 1 collagen scaffold, cut out and prepared as described in study 1. The scaffolds were 5 mm in diameter, and 1×10^6 cells were seeded on each scaffold. At 48 h after cell seeding on the collagen scaffolds, the animals were inoculated with tumor cell-seeded scaffolds. The skin was cut open on the right flank of Fox1$^{nu/nu}$ female nude mice, and the scaffold was placed under the skin.

2.4.2. Local Treatment Administration

On day 10, all tumors were evaluated using a vernier caliper to calculate their volume, as described in study 1. For inclusion in the study, the tumor volume had to be in the range of 60–100 mm^3. The animals that did not meet this inclusion criterion were removed from the experiment, leading to a sample size reduction in some groups (see the Results Section 3.1).

Local treatment administration was performed on day 11. The animals were randomized by randomly choosing a cage (five animals each), and all animals in the chosen cage were given the same treatment. Dose calculation was performed on the assumption that each animal weighed 20 g. All animals were weighed prior to tumor inoculation.

All animals were treated on day 11. The tumor was first palpated and the skin over the tumor was cut open using a scalpel. The tumor was then incised and the pellet of pure CaS/HA material or DASH was placed in its center, without performing any excision of tumor tissue. In the cases where the pellet could not be inserted into the tumor, it was placed immediately beside the tumor. The skin was closed with stitches. Group 1 ($n = 8$) was the control group, and no material or doxorubicin was administered locally. The tumor was surgically exposed, such that the local treatment was the only differing factor between groups.

Group 2 ($n = 8$) was treated with implantation of a pellet consisting of CaS/HA. The pellets were created using the same materials and methods as described for study 1; however, the liquid component used was distilled water instead of iohexol. Group 3 was treated with the low-dose DASH, with the dose of doxorubicin corresponding to 1.3 mg/kg (total amount of 26 µg DOX per pellet). Group 4 was treated with the intermediate-dose DASH, with doxorubicin dose corresponding to 3.9 mg/kg (total dose of 79 µg DOX per pellet). Group 5 was treated with the high-dose DASH, with the DOX dose corresponding to 10 mg/kg (total dose of 200 µg DOX per pellet).

2.4.3. Systemic Treatment Administration

All groups were treated with the systemic MAP treatment. The time points of the cycles and doses of all three drugs were the same for all groups. The animals received two cycles of intravenous MAP treatment. The first cycle started on day 13, while the second cycle started on day 22 after tumor inoculation. The drugs were administered in the lateral tail vein. The MAP dosage schedule is detailed below.

- Doxorubicin: 5 mg/kg (100 µg) once per cycle for 2 cycles, totaling 10 mg/kg (200 µg). Given on days 13 and 22.
- Cisplatin: 3 mg/kg (60 µg) once per cycle for 2 cycles, totaling 6 mg/kg (120 µg). Given on days 13 and 22.
- Methotrexate: 10 mg/kg (200 µg) once per cycle for 2 cycles, totaling 20 mg/kg (400 µg). Given on days 16 and 25.

2.4.4. Evaluation of Treatment Response Using PET-CT, Tumor Volume, Tumor Weight and Histology

PET-CT imaging was performed on day 31 or 32, as the terminal time point for treatment evaluation, at which point the metabolically active tumor volume was quantified. The PET-CT images were procured using the same machine, materials and methods as described above in study 1. The CT images acquired during the scan were used to verify the anatomical location of the PET signal. The total injected activity, tracer decay before starting the scan and volume of the region of interest were documented and used for the calculations of the PET-CT-based tracer uptake.

The animals were euthanized once the PET-CT reconstructed images were deemed to be of satisfactory quality. The animals were weighed and measurement of tumor dimensions and tumor volume was performed on the day the treatment was started, followed by one measurement every week until sacrifice at week 3, using the methods and materials as described in study 1, with the measurements serving as secondary outcome variables. All tumors were carefully excised after euthanization and digital photographs of each tumor were taken. This also applies to the histology methodology used in this study. The tumors were prepared as described in study 1; however, the samples were not decalcified before embedding in paraffin.

2.5. Statistics

The sample size was empirically calculated based on our previous studies utilizing similar experimental animal models [28,37,38]. The statistical analysis was performed using GraphPad Prism version 10.1. For the first study, the group data were first analyzed for normal distribution using the Shapiro–Wilk test. As some of the group data were not normally distributed, a non-parametric ANOVA (Kruskal–Wallis test) was applied. First, G2 (systemic doxorubicin) was chosen as the control group and the other groups were tested against it via Kruskal–Wallis analysis with Dunn's post hoc test. For a second analysis, G2 was excluded and, in a multivariate analysis, Kruskal–Wallis testing was performed for the remaining groups.

In the second study, the data distribution was first analyzed using the Shapiro–Wilk test. As all 5 groups passed the test, a parametric ANOVA was first performed to evaluate whether any statistical differences existed between the groups. Post hoc analysis was performed to compare treatment groups G2–G5 with the control group (G1) using Dunnett's test. Treatment groups G2–G5 were also compared between themselves using Tukey's multiple comparison post hoc test. In the case that a Gaussian distribution could not be observed, a non-parametric ANOVA (Kruskal–Wallis test) was used to determine statistical differences between the 5 groups. When differences were observed, Dunn's post hoc test was performed to compare groups G2–G5 to group G1, as well as to compare G2–G5 separately. Statistical significance was set at $p < 0.05$. All data are presented as mean ± SEM, unless otherwise stated.

2.6. Animal Ethics Statement

Animal experiments were performed using 4–5-week-old Fox1$^{nu/nu}$ female nude mice, purchased from Janvier Labs, Le Genest-Saint-Isle, France. They were maintained in cages in 12 h light/dark cycles. Animals were housed at the biomedical center, BMC, Lund University, and all institutional guidelines pertaining to animal care were followed. Animals were checked for signs of pain, wounds and general malaise three to four times a week. Humane endpoints included limping, pain or kyphotic body posture. The studies were performed in accordance with the ARRIVE guidelines, and the study protocol was approved by Jordbruksverket with the ethical approval number 5.8.18–01018/2020.

3. Results

3.1. Study 1

Two samples (in G4 and G3, one each) were excluded from all analyses, as no tumor was noted at the treatment time point and no signs of destruction were visible on micro-CT. Due to malfunction of the PET-CT scanner, the first four scanned animals belonging to G6 had to be excluded from the calculations. Three animals in G3 were excluded from the analysis, as two of them showed no spread of the tracer from the peritoneal cavity; this may have been caused by a faulty injection into the internal organs, rather than the peritoneal cavity. For the remaining analyses, all animals in all groups ($n = 8$, except for G3 and G4 ($n = 7$)) were included.

3.1.1. Analysis of Osteolysis in the Proximal Tibia Using Micro-CT

The 143b cells used for tumor inoculation are known to cause osteolysis, a secondary outcome marker of tumor progression. An overview of one representative animal from each group is shown in Figure 3A. All samples were classified into one of three degrees of bone destruction, based on a visual interpretation of the images; namely, either no destruction (intact cortex, no signs of resorption), low cortical destruction (signs of resorption present and some remaining tissue in the metaphysis, but not a complete cortex) or high cortical destruction (the cortex destroyed in the metaphysis and completely missing) (summarized in Figure 3B). For detailed micro-CT imaging results for each specimen, see the Supplementary Materials (Figures S1–S7).

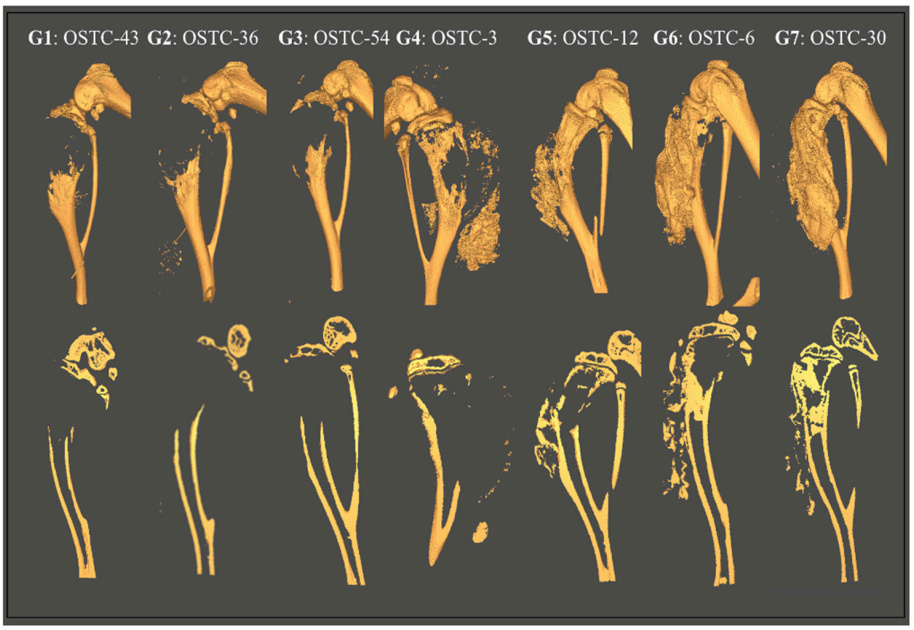
For G1 mice, which were treated with saline injections, all samples displayed significant bone destruction (Figure 3A). The epiphysis was intact; however, the tissue of the metaphysis and the proximal part of the diaphysis were missing, leading to the classification of high cortical destruction (Figure 3B). The cortex was destroyed in all except one sample, where some cortex was remaining, thus being classified as low cortical destruction (Figure 3B). Similar results were observed for G2 mice.

G3 mice also displayed a high level of destruction in the proximal tibia (Figure 3A). One sample in G3 was classified as low cortical destruction (Figure 3B). G4 mice showed greater variation in the amount of destruction (Figure 3B). Four of the seven samples had a similar amount and pattern of destruction as the previously described groups, thus being classified as high cortical destruction. One specimen had signs of resorption but intact cortices and was classified as low cortical destruction. For these samples, most of the material was pushed out into the surrounding tissue. Two samples had intact cortices, no signs of tissue destruction and the material was still in the medullary canal, and thus, were classified as no destruction (Figure 3B).

For G5 mice, treated with low-dose DOX delivered via the CaS/HA material, variable amount of bone destruction was observed. Four samples were classified as high cortical destruction; three samples had destruction surrounding the inoculation point but most of the cortices remaining in the metaphysis and, for two of those samples, the material was retained in the medullary canal, thus leading to their classification as low cortical destruction (Figure 3B). One sample had no signs of resorption and no loss of bone tissue, and thus, was classified as no destruction (Figure 3B).

G6 mice, which were treated with intermediate-dose DASH, also showed variations in the amount of bone tissue resorption (Figure 3B). One sample had extensive destruction and was classified as high cortical destruction. Four samples had a shorter diastasis and the destruction was less extensive, thus being classified as low cortical destruction (Figure 3B). The implanted material was also contained in the medullary canal for all but two samples. Three samples had intact cortices, and were classified as no destruction, with material remaining in the medullary canal (Figure 3B).

(A)



(B)

Group (*n*: Number of animals in the group)	No Destruction	Low Cortical Destruction	High Cortical Destruction	Material Located in Medullary Canal
G1 (*n*=8)	0	1	7	
G2 (*n*=8)	0	1	7	
G3 (*n*=7)	0	1	6	
G4 (*n*=7)	2	1	4	2
G5 (*n*=8)	1	3	4	3
G6 (*n*=8)	3	4	1	6
G7 (*n*=8)	6	2	0	8

Figure 3. Micro-CT-based evaluation of tumor-induced osteolysis. (**A**) Representative micro-CT specimens at the 2-week post-treatment time point. (**B**) Systematic overview of the number of animals in each group classified according to the degree of bone destruction evaluated using CT. Each animal is classified, based on a visual interpretation of the micro-CT imaging, as either No destruction (intact cortex, no signs of resorption), low cortical destruction (signs of resorption present and some remaining tissue in the metaphysis, but not a complete cortex) or high cortical destruction (the cortex destroyed in the metaphysis and completely missing). Group clarification: G1, treated with intratumoral saline injection; G2, treated with intravenous DOX (40 μg); G3, treated with intratumoral DOX injection (40 μg); G4, treated with intratumoral CaS/HA pellet (excipient); G5, treated with low-dose DASH (DOX-loaded CaS/HA pellet, 40 μg); G6, treated with intermediate-dose DASH (DOX-loaded CaS/HA pellet, 150 μg); G7, treated with high-dose DASH (DOX-loaded CaS/HA pellet, 300 μg).

G7 mice, treated with high-dose DASH, showed more consistent results, with six out of eight samples having intact cortices and the material retained in the medullary canal. As such, they were classified as no destruction (Figure 3A,B). Two of the eight samples presented destruction in the metaphysis and the cortices were missing in this area, but the diastasis from epiphysis to the remaining cortex was shorter compared with G1, G2 and the other groups, with extensive loss of bone tissue in the metaphysis, therefore leading to the classification of low cortical destruction (Figure 3B). The bone tissue was the most intact in this group and the material was retained in the medullary canal for all samples.

The destruction was therefore less extensive in the groups treated with DASH and showed a tendency to decrease with increasing DOX dosage.

3.1.2. Analysis of Metabolically Active Tumor in Proximal Tibia Using PET-CT

The tumors in G1 mice (saline-treated) had the highest mean value of % of injected activity (Figure 4A), which was significantly higher than those in G5 (low-dose DASH; $p < 0.01$) and G7 (high-dose DASH; $p < 0.0001$). G5 and G7 mice had similarly significantly lower tumor activity, measured as % of injected activity, when compared with those in G2 with systemic treatment of DOX ($p < 0.05$ and 0.0001, respectively). G7 mice (high-dose DASH) had significantly lower tumor activity than G3 mice (locally injected DOX) and G4 mice (carrier without DOX). PET-CT images for all animals are provided in the Supplementary Materials (Figures S8–S14).

3.1.3. Tumor Volume and Size

A collage of full body-pictures of one mouse from each group, representative of tumor size can be seen in Figure 4B(I). The average tumor volumes in G1 (treated with intratumoral saline) and G2 (treated with intravenous DOX) mice were 397 and 485 mm^3, respectively. G3 (treated with intratumoral DOX) and G4 (treated with excipient) mice had average volumes of 280 and 207 mm^3, respectively. G5 (low-dose DASH), G6 (intermediate-dose DASH) and G7 (high-dose DASH) mice had average volumes of 167, 81 and 58 mm^3, respectively. Mice in the three groups treated with CaS/HA and doxorubicin (G5, G6 and G7) had statistically significant smaller tumor volumes than those in the systemic doxorubicin-treated group, G2 (Figure 4B(IIa)). G7 mice also had significantly smaller tumor volumes than G1 mice (Figure 4B(IIa)). When comparing the average tumor weight, G6 and G7 mice had statistically significantly lower weight compared with systemic DOX-treated mice (G2) and those locally administered a saline injection (G1) (Figure 4B(IIb)).

3.1.4. Histology

All animals in G1 (treated with intratumoral saline) and G2 (treated with systemic DOX, 40 μg) demonstrated large tumors with bone destruction (Figure 5). For most sections, a necrotic core was present in the cancerous tissue. G3 mice (treated with intratumoral DOX, 40 μg) had a similar appearance, with large tumors situated between and amidst the destructed tibia. Only the epiphysis remained in the proximal tibia for most sections in these groups. Two animals in G4 (treated with excipient only) had no signs of cancer presence, showing intact cortices surrounded by skeletal muscle. However, the remaining animals had large tumors with a necrotic core and bone destruction.

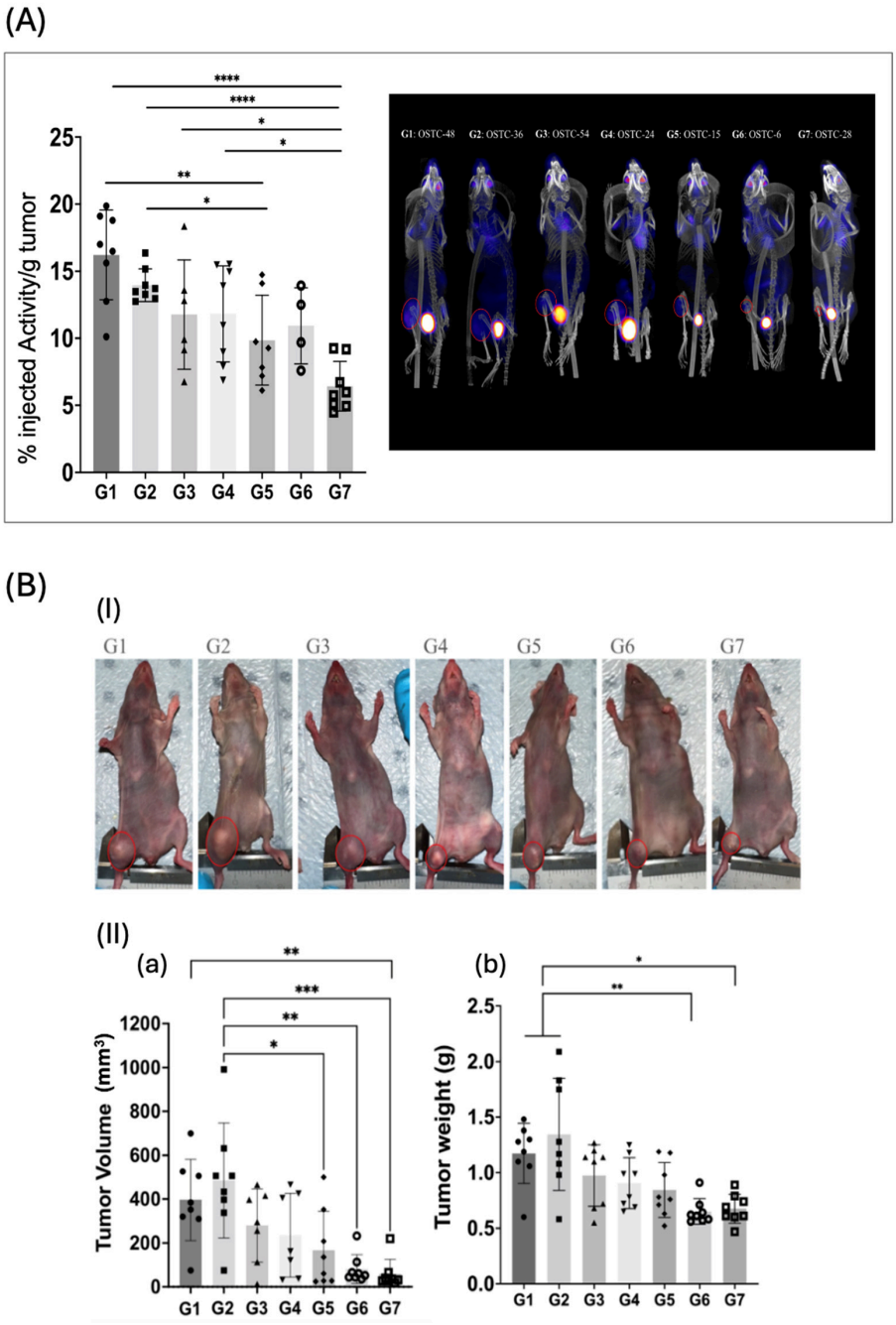


Figure 4. Terminal time point evaluation of treatment response using in vivo PET-CT and ex vivo tumor volume and weight calculations. The graph in panel (**A**) demonstrates tumor activity, measured as % of injected activity per gram of tumor tissue. * p-value < 0.05, ** $p < 0.01$ and **** $p < 0.0001$. Collage of PET-CT images (right) taken at 3 weeks after treatment initiation, with one representative animal from each treatment group. (**B**) Panel (**I**) shows a collage of full-body pictures of one mouse from each group, with representative tumor size. (**II**). Calculation of tumor volume (left) and tumor weight (right) at the study endpoint of 3 weeks. The graphs in the figure present data as the mean ± SD of the tumor volume (**a**) or weight (**b**). * p-value < 0.05, ** $p < 0.01$, *** $p < 0.001$. Data were not normally distributed, and the statistical analysis was performed using a Kruskal–Wallis test with Dunn's post hoc test. G2 mice (i.e., those receiving systemically administered DOX) were used as controls during multiple comparisons testing. Group clarification: G1, treated with intratumoral saline injection; G2, treated with intravenous DOX (40 µg); G3, treated with intratumoral DOX injection (40 µg); G4, treated with intratumoral CaS/HA-pellet (excipient); G5, treated with low-dose DASH (DOX-loaded CaS/HA pellet, 40 µg); G6, treated with intermediate-dose DASH (DOX-loaded CaS/HA pellet, 150 µg); G7, treated with high-dose DASH (DOX-loaded CaS/HA pellet, 300 µg).

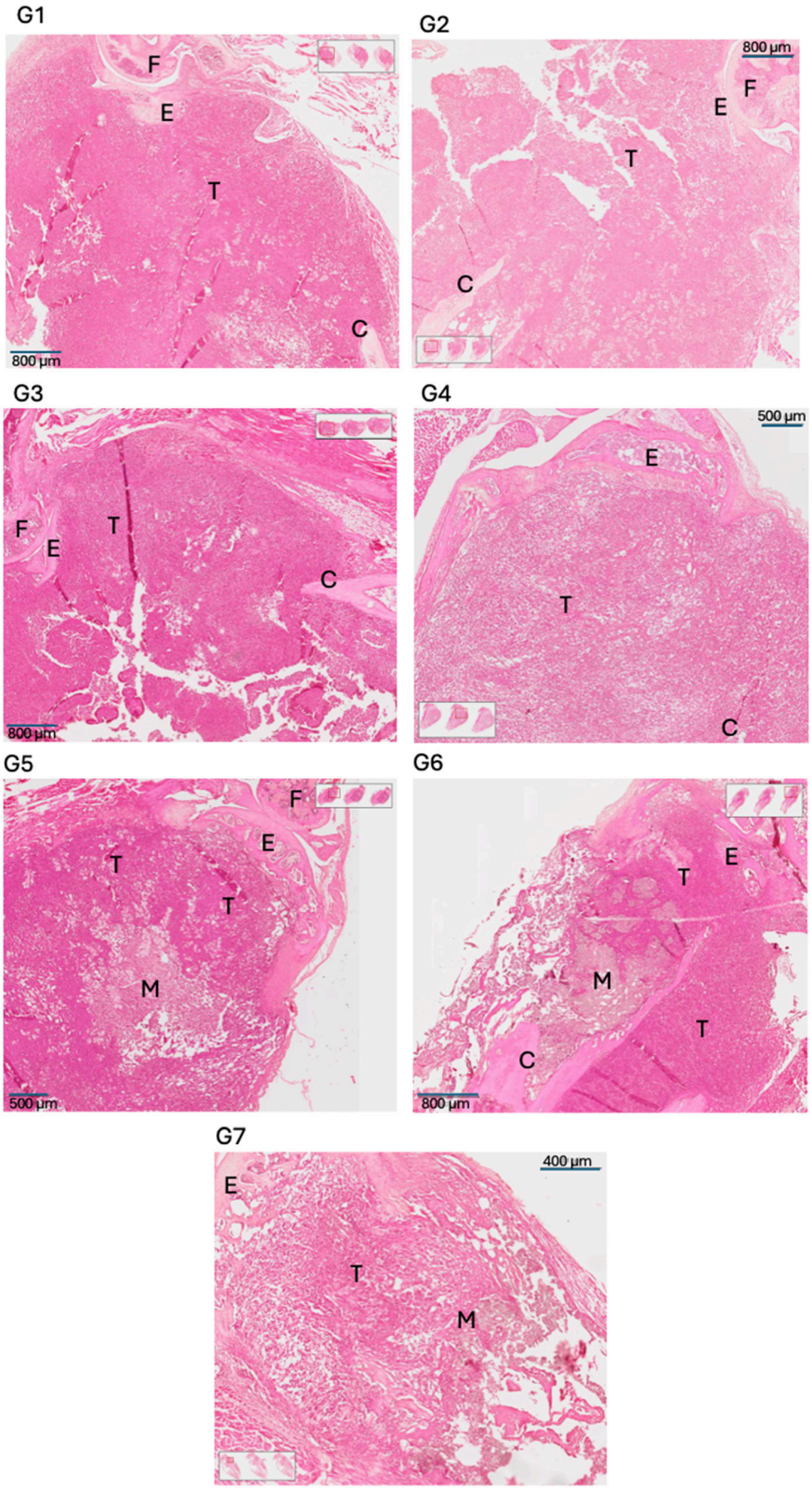


Figure 5. Histological slides for one representative animal from each group. Group clarification: G1, treated with intratumoral saline injection; G2, treated with intravenous DOX (40 µg); G3, treated with intratumoral DOX injection (40 µg); G4, treated with intratumoral CaS/HA pellet (excipient); G5, treated with low-dose DASH (DOX-loaded CaS/HA pellet, 40 µg); G6, treated with intermediate-dose DASH (DOX-loaded CaS/HA pellet, 150 µg); G7, treated with high-dose DASH (DOX-loaded CaS/HA pellet, 300 µg). Histological landmarks are marked out with letters: F—femur, E—epiphysis, C—cortex, M—material (excipient or DASH), T—tumor tissue.

Of the G5 mice (treated with low-dose DASH, 40 µg), four animals displayed similar progression as the previous groups, with excipient material (gray-pink in color) dispersed in the center. Two animals had tumor tissue located as a nest in the medullary canal, almost contained by the cortices who displayed local destruction. One animal had tumor tissue at the inoculation point, as well as surrounding the proximal tibia; although it was lesser in size than previous groups, and extensive bone destruction was still present. One animal showed no presence of cancerous tissue. Of the animals treated with intermediate-dose DASH (150 µg), two animals showed large amounts of tumor, similar to groups 1, 2 and 3 regarding progression. In contrast, three animals had smaller nests of tumor cell tissue maintained at the inoculation point, and two animals had no visual tumor tissue with intact cortices surrounded by skeletal muscle. In G7 (treated with high-dose DOX, 300 µg), two animals had extensive tumors surrounding the tibia with bone destruction; three animals had no nests of tumor tissue and no bone destruction; and the remaining three animals had small nests of tumor tissue at the inoculation point contained by the cortices and excipient material. Bone tissue destruction was less extensive than that in animals in groups 1, 2 and 3.

3.2. Study 2

A total of $n = 3$ animals had to be excluded from the experiment, as they did not fulfill the inclusion criterion due to a tumor volume <60 mm^3. These animals comprised one each in groups 1, 2 and 5. Furthermore, one animal in group 3 and one animal in group 4 were lost during the i.v. injections on day 13. A total of $n = 8$ animals in each experimental group completed the entire experiment.

Animal randomization was performed based on cages and not individual animals. One out of nine possible cages was randomly chosen. Post hoc statistical analysis revealed no differences in the initial tumor volume (i.e., tumor volume at day 10) between the five treatment groups except in group 2, which had a lower mean tumor volume compared with group 1, as detailed in the Supplementary Materials (Figure S15). No statistically significant differences were observed in animal weight at the start of the treatment period.

3.2.1. Tumor Volume and Size

On the treatment day, the animals' weight, tumor dimensions and tumor volume were measured, followed by one measurement every week until sacrifice at week 3 (Figure 6A). Regarding weight changes, no significant differences in weight were observed at any of the measurement time points (Figure 6A). In contrast, significant differences in tumor volume were observed at each time point, as detailed in Table 2 below.

Table 2. Longitudinal tumor volume assessment, presented as mean ± SEM (in mm^3).

Time Point	Treatment Groups					Statistics
	MAP	**MAP + Excipients**	**MAP + DASH (26 µg)**	**MAP + DASH (79 µg)**	**MAP + DASH (199 µg)**	
Week 0	79 ± 4	64 ± 1	75 ± 4	70 ± 2	67 ± 3	MAP vs. MAP + Excipients $p < 0.01$
Week 1	109 ± 11	113 ± 18	54 ± 20	35 ± 4	23 ± 6	a. MAP vs. MAP + DASH (79 µg) $p < 0.05$ b. MAP vs. MAP + DASH (199 µg) $p < 0.001$ c. MAP + Excipients vs. MAP + DASH (199 µg) $p < 0.01$

Table 2. *Cont.*

Time Point	Treatment Groups					Statistics
	MAP	**MAP + Excipients**	**MAP + DASH (26 µg)**	**MAP + DASH (79 µg)**	**MAP + DASH (199 µg)**	
Week 2	313 ± 52	274 ± 36	107 ± 49	46 ± 11	31 ± 6	a. MAP vs. MAP + DASH (79 µg) $p < 0.01$ b. MAP vs. MAP + DASH (199 µg) $p < 0.001$ c. MAP + Excipients vs. MAP + DASH (79 µg) $p < 0.01$ d. MAP + Excipients vs. MAP + DASH (199 µg) $p < 0.001$
Week 3	701 ± 81	683 ± 67	170 ± 93	68 ± 10	32 ± 4	a. MAP vs. MAP + DASH (26 µg) $p < 0.01$ b. MAP vs. MAP + DASH (79 µg) $p < 0.01$ c. MAP vs. MAP + DASH (199 µg) $p < 0.001$ d. MAP + Excipients vs. MAP + DASH (79 µg) $p < 0.05$ e. MAP + Excipients vs. MAP + DASH (199 µg) $p < 0.0001$

In the post-mortem analysis, tumor dimensions were measured using a vernier caliper. All tumors were carefully excised and a digital photograph of each tumor was taken (Figure 6B). All MAP + DASH specimens had statistically lower tumor volumes when compared with MAP-only specimens (Figure 6B). This reduction in tumor volume was dependent on the DOX dose, with the lowest tumor volume observed in the MAP + DASH (199 µg) group (Figure 6B). Furthermore, the volumes in the MAP + DASH (79 µg) ($p < 0.05$) and MAP + DASH (199 µg) ($p < 0.0001$) groups were also significantly lower than that in the MAP + Excipients group (Figure 6B). Similar trends were observed for tumor weight. All MAP + DASH groups had significantly lower tumor weight compared with the MAP control group. The MAP + DASH (26 µg) and MAP + DASH (199 µg) groups also had significantly lower tumor weights than the MAP + Excipients group (Figure 6B).

3.2.2. PET-CT

Regarding normalized tracer uptake (Figure 7, top left), the MAP + DASH (199 µg) group mice showed the lowest tracer uptake, which was also statistically significant when compared with that in the control MAP group ($p < 0.05$). On the other hand, MAP + Excipients group mice had significantly higher tracer uptake than the MAP group mice ($p < 0.05$). All MAP + DASH group mice had significantly lower normalized tracer uptake, when compared with MAP + Excipients group mice.

When looking at the total intratumoral uptake of the radioactive tracer (i.e., the % of radioactivity detected in the tumor with respect to the total injected radioactivity) (Figure 7, top middle), MAP + DASH (26 µg) ($p < 0.01$) and MAP + DASH (199 µg) ($p < 0.01$) mice showed significantly lower tracer uptake when compared with MAP-only mice. MAP + DASH (79 µg) mice, although demonstrating low tracer uptake, did not reach a statistically significant difference ($p = 0.07$). Between the DASH groups, MAP + DASH (199 µg) ($p < 0.001$), as well as MAP + DASH (26 µg) ($p < 0.01$) mice demonstrated significantly lower tracer uptake in comparison with MAP + Excipients group mice. PET-CT-based

tumor volume (i.e., the volume of the region of interest used to quantify the uptake of the radioactive tracer) was also quantified (Figure 7, top right). All MAP + DASH group mice showed significantly lower tumor volumes when compared with the control MAP group mice ($p < 0.01$). All MAP + DASH group mice also showed significantly lower volume than those in the MAP + Excipients group, with volume reducing with increasing DOX dose. Tracer uptake quantification also corroborated the conclusions derived from PET-CT images. The MAP and MAP + Excipients group mice had the largest tumor tissue and highest uptake. The MAP + DASH (26 µg) and MAP + DASH (79 µg) group mice demonstrated some 18 F-FDG uptake, but at a lower level than those in the MAP and MAP + Excipients groups. Finally, very little to no tracer activity was observed in the MAP + DASH (199 µg) group mice. Remnants of the CaS/HA material were observed in all MAP + DASH groups.

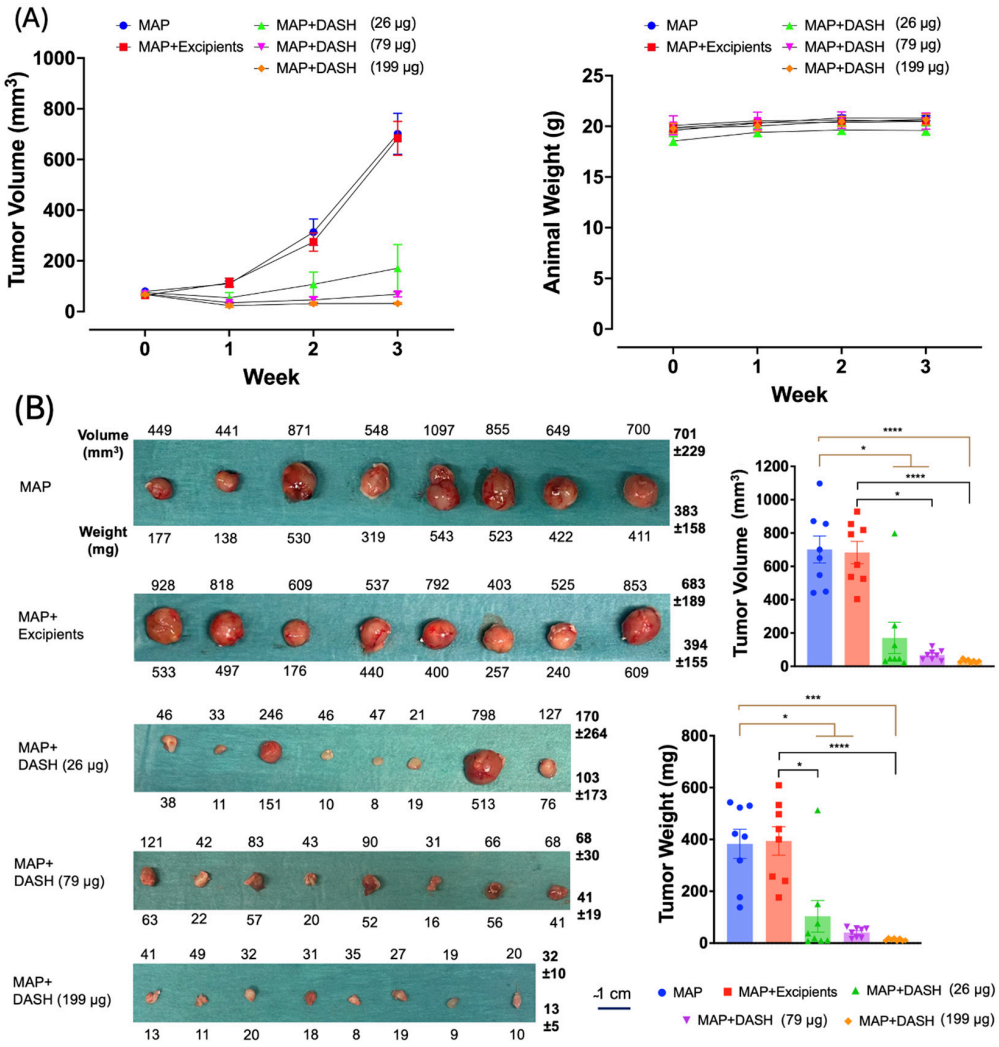


Figure 6. Tumor volume and weight measurements in study 2. (**A**) Longitudinal assessment of tumor volume progression in different treatment groups (left), as well as animal weight changes over time (right). (**B**) Post-mortem analysis of tumor tissue. Digital photographs on the left show excised tumors at three weeks after treatment. Each tumor represents tissue harvested from one individual animal. The graph on the top right shows tumor volume measurements performed before the tissue was excised from the animals. The graph on the bottom right shows tumor weight at the time of sacrifice. Statistical comparisons with brown bars indicate comparison of the treatment groups G2–G5 with respect to the control MAP-only group (G1). Black bars indicate comparisons between the treatment groups G2–G5. * $p < 0.05$, *** $p < 0.001$ and **** $p < 0.0001$. Statistical significance was set at $p < 0.05$.

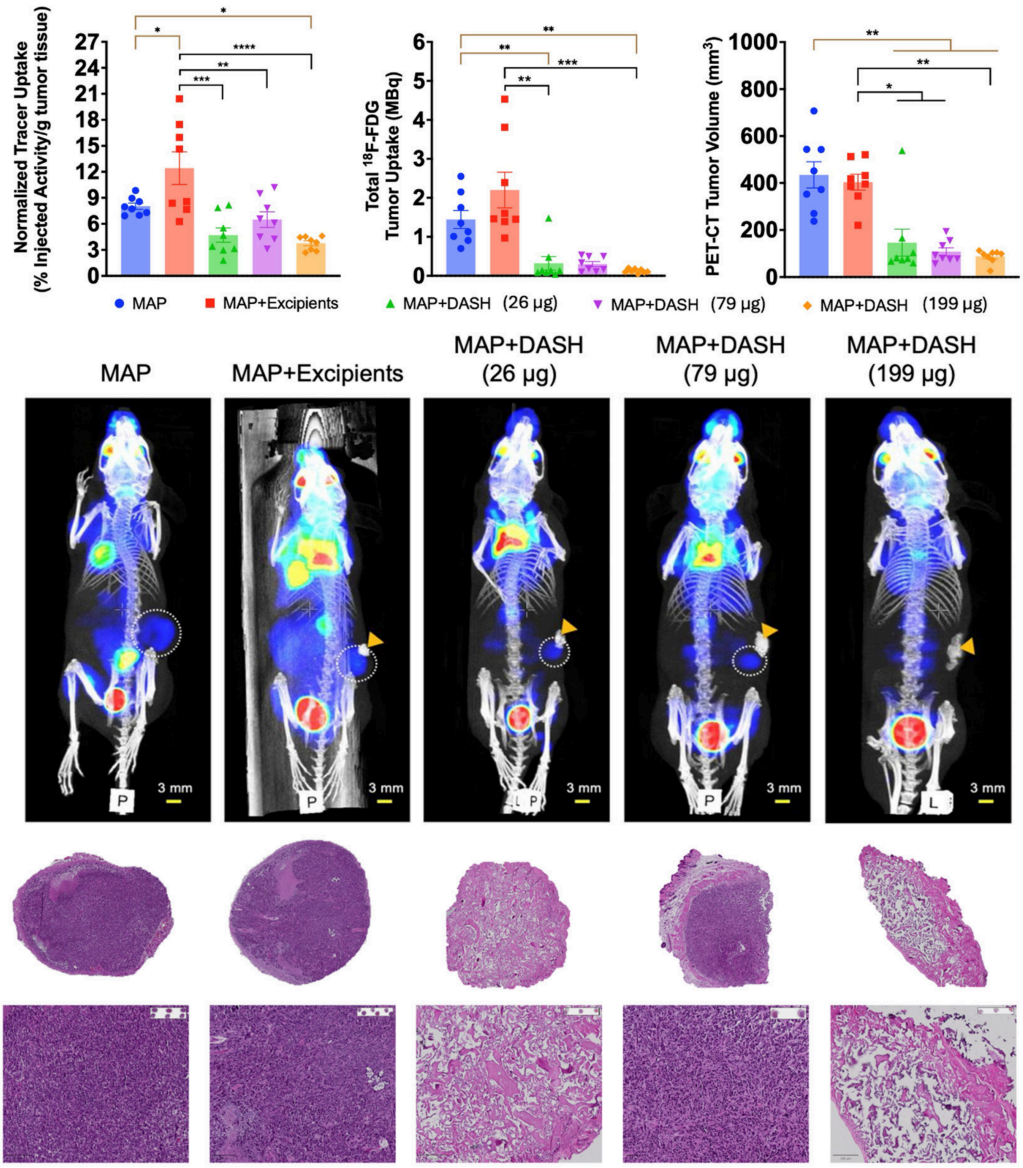


Figure 7. PET-CT and histological responses in study 2. PET-CT imaging provided quantitative data on treatment response. The top left graph represents normalized tracer uptake in each treatment group as a % of total injected radioactivity/g tumor tissue. The middle graph shows total tracer uptake without normalizing against tumor weight and, finally, the graph on the right shows the PET-CT-based tumor volume used to quantify the data in the graphs in the left and middle panels. Statistical comparisons with brown bars indicate comparison of treatment groups G2–G5 with respect to the control MAP-only group (G1); black bars indicate comparisons between the treatment groups G2–G5. * $p < 0.05$, ** $p < 0.01$, *** $p < 0.001$ and **** $p < 0.0001$. Statistical significance was set at $p < 0.05$. Images in the middle row present one representative PET and CT overlapped image from each treatment group. Images were assigned a threshold manually to provide a similar color scale. The tumor and the tracer uptake area in the tumor are marked with a dashed white circle, while the orange arrow in groups G2–G5 indicates the radio-dense DASH excipients. The bottom row shows representative histology slides for one animal from each treatment group.

3.2.3. Histology

The G1 (MAP-only treatment) and G2 (MAP + excipient-treated) animals presented visible cancer cells (Figure 7). Specimens in these groups consisted entirely of dense cancer cell tissue. G3 animals (treated with MAP + low-dose DASH) had mixed constituency, with three out of eight animals having preparations showing densely packed cancer tissue,

similarly to G1 and G2 mice; however, the other samples demonstrated tumors with fibrotic tissue and no clearly visible nests of cancer cells. In G4 (MAP + intermediate-dose DASH) animals, five out of eight specimens showed dense cancer cell tissue and the other three showed fibrotic tissue with no clear nests of cancer cells. One of the specimens consisted mainly of adipose tissue. In the samples from the animals treated with MAP + high-dose DASH (G5), no visible cancer cell tissue could be seen. The preparations had fibrotic tissue and necrosis in the center. Dispersed cancer cells were difficult to ascertain in the samples with fibrotic appearance.

3.2.4. Local Tissue Reaction at the DASH Implantation Site

The calcium sulfate component in DASH can cause delayed wound-healing. Likewise, DOX extravasation into connective tissue during intravenous administration can cause local tissue inflammation and necrosis. The local tissue reactions to MAP-excipients (group 2) and DASH containing various DOX doses (G3–G5) are shown in Figure 8. As expected, the MAP group mice showed no local tissue reaction. In the case of the MAP + Excipients and MAP + DASH (26 µg) groups, 1 out of 8 animals demonstrated notable delayed wound-healing and scar tissue formation. This increased slightly with an increase in DOX dose, with 3/8 and 2/8 animals demonstrating scar tissue formation in the MAP + DASH (79 µg) and MAP + DASH (199 µg) groups, respectively.

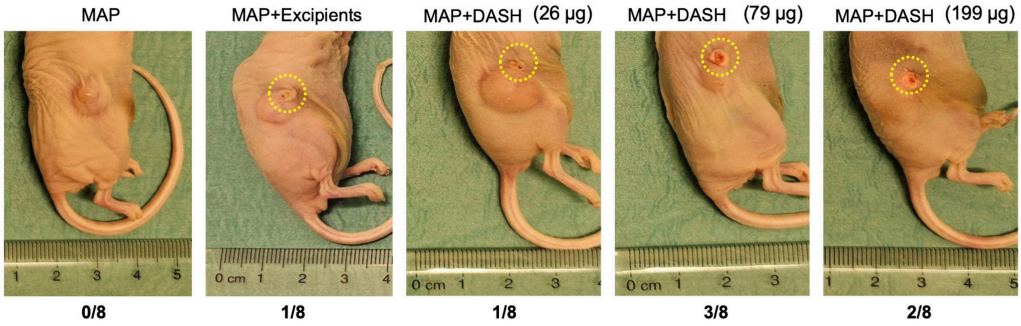


Figure 8. Local tissue reaction at the site of DASH implantation at 3 weeks post-implantation. Dashed yellow circle highlights the area of interest in each group.

4. Discussion

This study aimed to evaluate the ability of DASH to improve local disease control in an orthotopic osteosarcoma model in nude mice, as well as to evaluate its safety and efficacy as an add-on to systemically administered MAP in a sub-cutaneous osteosarcoma model in nude mice.

In the orthotopic study, DASH-treated mice demonstrated an increased treatment response, regarding the primary and secondary outcomes, when compared with systemic doxorubicin. The visual interpretation of the tumor size on PET imaging aligned with the extent of bone destruction seen on micro-CT imaging, histology and, more importantly, the tumor volume and weight calculations. The systemic treatment did not significantly hinder tumor growth or bone destruction, resulting in a treatment response similar to that to intra-tumoral saline injection.

In the subcutaneous study, the tumor volume, weight and tumor activity (measured as % injected activity) results were in good concordance. A reduction in tumor burden and an increase in tumor-inhibiting ability was seen in the MAP + DASH groups compared with MAP control group, except that regarding tumor activity with MAP + DASH (79 µg), which was not statistically significantly lower than that in controls.

Similar to study 1, the treatment effect in study 2 presented a dose-dependent trend. Although no statistically significant difference in treatment response was observed with respect to the different DASH doses used, increased treatment response was associated with higher doses of DOX loaded on DASH. This was demonstrated in the primary and secondary outcomes in regard to study 1, with the tumors in the high-dose (300 µg) group being smaller, lighter and less metabolically active when compared with those in the low- and intermediate-dose (40 µg and 150 µg) groups. Similarly, in study 2, little to no tracer activity was observed in the MAP + DASH (199 µg) group mice.

Considering that the average weight of a nude mouse is 20 g, the DOX dose in the 199 µg group in study 2 was equivalent to 10 mg/kg. In a study performed by Chen et al., tumor-bearing nude mice were treated with three concentrations of doxorubicin, locally delivered via a PLGA-PEG-PLGA hydrogel [39]. Mice treated with 5 mg/kg DOX locally showed no systemic toxic effects; however, this dose had no effect on tumor suppression. In mice treated with 30 mg/kg, great tumor-killing ability of DOX was observed, but the mice also suffered from weight loss. Those in the intermediate group, with a dose of 15 mg/kg DOX, showed evidence of a significant tumor-impeding ability and lived significantly longer compared with those systemically administered DOX at the same dosage. Therefore, an important aspect is to ascertain not only the amount of DOX that is safe to deliver but also the applicability of the platform to provide local disease control and potential metastasis prevention.

As no detrimental side-effects of high local DOX delivery were observed in this short-term study, the results indicate that either only a fraction of the DOX reaches the systemic circulation or the exposure is gradual. Aston et al. have demonstrated that the maximum tolerated dose of doxorubicin in nude mice is 10 mg/kg [40]. The high-dose group in the second study received high local DOX (10 mg/kg), as well as systemically administered DOX, thus putting these mice above the 10 mg/kg limit; however, they all survived without substantial weight loss. This may imply the ability of DASH to maintain the DOX concentration locally and a lack of synergistic systemic toxicity effects between the local and systemic treatment modalities. Systemic toxicity and side effects such as heart failure and myeloid suppression are dose-limiting factors for DOX. However, it must be noted that we only performed a short-term follow-up, and the long-term safety of the tested regimen remains unknown.

Regarding the local toxicity, no scar tissue formation was observed in the control group in the subcutaneous study. In the MAP + excipient and MAP + low dose DASH groups, one animal per group demonstrated scar formation, and an increase in the number of animals presenting scar tissue was seen with an increase in the DOX dosage. Due to the small size of the experimental groups, it is difficult to conclude whether the formation of scar tissue is due to the implantation of excipients or exposure to high doses of DOX. More experiments are required to elucidate the local tissue reaction to DASH at the implantation site.

In the second study, the MAP + DASH (26 µg) and MAP + DASH (199 µg) group mice had statistically lower tumor weights and % injected tumor activity than those in the MAP + excipients group. Furthermore, the MAP + DASH (79 µg) and MAP + DASH (199 µg) group mice had lower tumor volumes when compared with those in the MAP + excipients group. The inhibiting effect of DASH compared with excipient in both studies provides evidence for DOX acting as the primary tumor inhibitor in the platform. In a study performed by Zhang et al., hydroxyapatite itself was shown to have a combined functionality of possessing tumor cytotoxic abilities and acting as a bone segmental defect filler after tumor invasion [41]. In study 1, one group of mice was administered DOX intratumorally (40 µg), but this treatment did not demonstrate statistically significant tumor-inhibiting

abilities. These results imply that the platform and DOX have synergistic effects, likely due to the prolonged release of DOX from DASH.

In study performed in 40 patients treated with a multi-agent neoadjuvant treatment followed by surgery, reductions in size and tumor growth in response to treatment were reported to be strongly associated with the degree of tumor necrosis, which was thus considered as a predictive factor [13]. Thus, the results of this study indicate that DASH could be implemented as part of a novel protocol for poor responders. A second predictive factor the abovementioned researchers investigated was an increase in osteoid tissue after treatment, serving as a positive predictor [13]. In this study, micro-CT and histology imaging revealed that the ceramic biomaterial appeared to be incorporated into cortical bone and stabilized the drilled cavity, when compared with non-DASH groups in which the diaphysis had undergone osteolysis. However, G4 mice—which were treated with only the material—still showed extensive destruction, indicating that the primary protector of bone from osteolysis was the pharmacological action of doxorubicin.

Similar studies investigating the tumor-inhibiting effects of DOX combined with HA in orthotopic and subcutaneous nude mice models inoculated with 143b cells have previously been performed by Yang et al. [28,38], in which the orthotopic model was developed to mimic a post-surgical scenario. These studies concluded an increased treatment response to DOX combined with HA, when compared with systemic DOX treatment. The collective results of these studies point to an increased ability of DOX loaded on an HA-based platform to inhibit tumor development in native and subcutaneous tissue pre-surgery and recurrence post-resection, indicating an opportunity to use the platform as an adjunct for poorly responding patients, or those showing low tolerance to systemic treatment. The risk for local recurrence is low in osteosarcoma, having been reported at 4–10% [42,43]; however, there are other cancer diseases—such as soft tissue sarcoma, breast, lung and colorectal cancer—with higher risk in this regard, for which a local suppressor could be an important adjuvant [44].

Other preclinical studies have explored the possibility of local delivery of cytostatics to treat malignant bone tumors; for example, Wang et al. developed cisplatin-loaded bone substitute granules [45]. In particular, they utilized and functionalized commercially available bone substitute granules such as Bio-Oss® and MBCP®+ with cisplatin, and delivered them to co-cultures of metastatic breast, prostate cancer and bone marrow stromal cells. The functionalized granules showed a dose-dependent cytotoxic effect on cancer cells and less impact on stromal cells. When the material was implanted in rat femoral condyles, no local tissue damage was observed and no apoptotic damage was seen in the liver or kidneys. Therefore, they were also able to demonstrate dose-dependent cytotoxicity and that bone substitute materials loaded with cytostatics can potentially be regarded as safe for application regarding their systemic effects. However, more extensive studies still need to be performed to elucidate the local toxicity of the materials proposed in this study, due to the increased scar tissue and wound formation observed in the mice administered higher doses of local DOX.

Our study has a few limitations. In study 1, a low volume of cell suspension was chosen for seeding the scaffolds, which caused some uncertainty; for example, it is suspected that two scaffolds which may not have carried viable cells were implanted (Supplementary Figure S16). During treatment, all animals were checked for tumors and all animals (except one) inoculated on day 1 carried a visible tumor at the initiation of treatment. It is possible that scar tissue could have been confused for tumor tissue, as the micro-CT scans, PET scans and tumor measurements could not confirm the presence of tumors in one animal each for the low treatment response groups G3 (OSTC-52) and G5 (OSTC-18), as well as two animals in G4 (OSTC-25 and -7). The animal in G3 (OSTC-52) had tumor tissue visible

on histology. In the remaining three animals, the presence of tumor tissue was difficult to ascertain. Nevertheless, all animals mentioned here were included in the micro-CT and PET-CT analyses, and all Micro-CT, PET-CT and histology images for these specimens are provided in the Supplementary Materials (Figures S1–S14 and S17).

Another possible explanation is that the tumors may have been in a nascent stage, at which even a limited treatment could have impeded their development; for example, two animals in G7 had a higher tumor burden than the remaining animals, which otherwise showed a very successful response. One of them was reported to already have a large tumor burden at treatment initiation compared with the others. Second, all animals in G1 and G2 underwent successful inoculation. To reduce the inter-animal variability in the second study, we performed tumor volume measurements before administering the treatments and set an inclusion criteria based on tumor size. Another limitation of our orthotopic study is the risk of observer bias in the classification of the bone destruction on Micro-CT 3D imaging, due to it not being performed by a blinded assessor. For transparency and to minimize the risk of observer bias, all obtained images are included in the Supplementary Materials.

Due to the aggressive nature of the used cell line, large tumors can form within short periods of time. In orthotopic studies, this entails short experimental setups due to painful and crippling tumors. This is a limitation of the study, as survival and remission in patients with localized disease are ultimately determined based on the development of metastasis. Models adapted to investigate metastatic progression and development should be employed as a next step. A suitable candidate for this purpose is the model developed by Martine et al., which was developed to investigate interactions between human bone cancer cells and engineered human bone tissue in vivo by implanting bioengineered scaffolds ectopically in immunodeficient hosts, enabling the development of larger tumors [46].

Another important factor to establish is the exposure to DOX over time, which correlates to the treatment effect and side-effects. The AUC and other pharmacokinetic properties can be calculated after taking regular blood samples over the treatment period. However, the required quantity of blood samples for such an analysis is difficult to obtain from mice. A study on the biodistribution of doxorubicin is therefore planned to be performed in sheep.

5. Conclusions

In an orthotopic bone tumor model, a local drug delivery platform delivering doxorubicin from a CaS/HA biomaterial was associated with a higher treatment response, reported as a greater impairment of tumor growth and bone destruction when compared with systemic treatment, which is currently used as the standard administration pathway for cytostatic agents in osteosarcoma patients. The addition of a local chemotherapeutic regimen to the MAP protocol, demonstrated increased tumor impediment as well as dose-dependent cytotoxicity. In the future, such a regimen could not only be considered for the development of an additive treatment for use in poor responders but also as a standard treatment modality against osteosarcoma as well as other solid tumors. However, pharmacokinetic studies in large animals and material characterizations need to be carried out before clinical translation would be possible.

Supplementary Materials: The following supporting information can be downloaded from https://www.mdpi.com/article/10.3390/cancers18223620/s1: Figure S1: Micro-CT imaging of the mice in G1; Figure S2: Micro-CT imaging of the mice in G2; Figure S3: Micro-CT imaging of the mice in G3; Figure S4: Micro-CT imaging of the mice in G4; Figure S5: Micro-CT imaging of the mice in G5; Figure S6: Micro-CT imaging of the mice in G6; Figure S7: Micro-CT imaging of the mice in G7; Figure S8: PET-CT imaging of the mice in G1; Figure S9: PET-CT imaging of the mice in G2; Figure S10: PET-CT imaging of the mice in G3; Figure S11: PET-CT imaging of the mice in G4; Figure S12: PET-CT imaging of the mice in G5; Figure S13: PET-CT imaging of the mice in G6; Figure S14: PET-CT imaging

of the mice in G7; Figure S15: Tumor volume at the start of the experiment in study 2; Figure S16: MTT assay results; Figure S17: Histology from specimen in low responsive groups with low tumor burden.

Author Contributions: All authors contributed to the research and the manuscript's development. Conceptualization, D.B.R., J.E., M.T., T.C., V.M., M.L. and L.L.; methodology, T.C., D.B.R., T.A., J.H. and H.A.; software, T.C., J.H. and D.B.R.; validation, D.B.R., T.C. and H.A.; formal analysis, T.C., T.A., J.H. and H.A.; investigation, T.C., J.E., M.T., D.B.R., M.L., V.M. and L.L.; resources, D.B.R., M.T. and L.L.; data curation, T.C., H.A. and J.H.; writing—original draft preparation, T.C.; writing—review and editing, T.C., D.B.R., H.A., J.H., M.T., T.A., L.L., M.L., V.M. and J.E.; visualization, T.C., T.A., J.H. and H.A.; supervision, D.B.R., M.T. and L.L.; project administration, T.C., D.B.R. and M.T.; funding acquisition, D.B.R. and M.T. All authors have read and agreed to the published version of the manuscript.

Funding: This research was funded by the Swfedish Research Council (2021-03447), Fru Berta Kamprad Foundation, Crafoord Foundation (2025-0884) and the Royal Physiographic Society, Lund.

Institutional Review Board Statement: The animal study protocol was approved by the Institutional Review Board of Jordbruksverket (protocol code 5.8.18–01018/2020, approved 18 January 2020) for studies involving animals.

Informed Consent Statement: Not applicable.

Data Availability Statement: All imaging and cell viability assay results can be viewed in the Supplementary Materials.

Acknowledgments: The authors thank the infrastructure support from Lund University, Sweden and the Lund Bioimaging Center (LBIC) at the Faculty of Medicine, Lund University, Sweden. The authors have reviewed and edited the output and take full responsibility for the content of this publication.

Conflicts of Interest: D.B.R., M.T. and L.L. hold stocks in Lithea, AB, Lund, Sweden. All other authors declare no competing interests.

Abbreviations

The following abbreviations are used in this manuscript:

OS	Osteosarcoma
DOX	Doxorubicin
HA	Hydroxyapatite
CaS/HA	Calcium-sulfate hydroxyapatite
DASH	Doxorubicin + calcium-sulfate hydroxyapatite
MAP	Methotrexate–adriamycin–cisplatin
PET	Positron emission tomography

References

1. Corre, I.; Verrecchia, F.; Crenn, V.; Redini, F.; Trichet, V. The osteosarcoma microenvironment: A complex but targetable ecosystem. *Cells* **2020**, *9*, 976. [CrossRef]
2. Mirabello, L.; Troisi, R.J.; Savage, S.A. International osteosarcoma incidence patterns in children and adolescents, middle ages and elderly persons. *Int. J. Cancer* **2009**, *125*, 229–234. [CrossRef]
3. Huvos, A.G. Osteogenic sarcoma of bones and soft tissues in older persons. A clinicopathologic analysis of 117 patients older than 60 years. *Cancer* **1986**, *57*, 1442–1449. [CrossRef]
4. Longhi, A.; Errani, C.; Gonzales-Arabio, D.; Ferrari, C.; Mercuri, M. Osteosarcoma in patients older than 65 years. *J. Clin. Oncol.* **2008**, *26*, 5368–5373. [CrossRef]
5. Marko, T.A.; Diessner, B.J.; Spector, L.G. Prevalence of metastasis at diagnosis of osteosarcoma: An international comparison. *Pediatr. Blood Cancer* **2016**, *63*, 1006–1011. [CrossRef]
6. Whelan, J.S.; Davis, L.E. Osteosarcoma, chondrosarcoma, and chordoma. *J. Clin. Oncol.* **2018**, *36*, 188–193. [CrossRef]
7. Allison, D.C.; Carney, S.C.; Ahlmann, E.R.; Hendifar, A.; Chawla, S.; Fedenko, A.; Angeles, C.; Menendez, L.R. A meta-analysis of osteosarcoma outcomes in the modern medical era. *Sarcoma* **2012**, *2012*, 704872. [CrossRef]

8. Smeland, S.; Bielack, S.S.; Whelan, J.; Bernstein, M.; Hogendoorn, P.; Krailo, M.D.; Gorlick, R.; Janeway, K.A.; Ingleby, F.C.; Anninga, J.; et al. Survival and prognosis with osteosarcoma: Outcomes in more than 2000 patients in the EURAMOS-1 (European and American Osteosarcoma Study) cohort. *Eur. J. Cancer* **2019**, *109*, 36–50. [CrossRef]
9. Kansara, M.; Teng, M.W.; Smyth, M.J.; Thomas, D.M. Translational biology of osteosarcoma. *Nat. Rev. Cancer* **2014**, *14*, 722–735. [CrossRef]
10. Bacci, G.; Ferrari, S.; Bertoni, F.; Ruggieri, P.; Picci, P.; Longhi, A.; Casadei, R.; Fabbri, N.; Forni, C.; Versari, M.; et al. Long-term outcome for patients with nonmetastatic osteosarcoma of the extremity treated at the istituto ortopedico rizzoli according to the istituto ortopedico rizzoli/osteosarcoma-2 protocol: An updated report. *J. Clin. Oncol.* **2000**, *18*, 4016–4027. [CrossRef]
11. Bacci, G.; Longhi, A.; Fagioli, F.; Briccoli, A.; Versari, M.; Picci, P. Adjuvant and neoadjuvant chemotherapy for osteosarcoma of the extremities: 27 year experience at Rizzoli Institute, Italy. *Eur. J. Cancer* **2005**, *41*, 2836–2845. [CrossRef]
12. Spraker-Perlman, H.L.; Barkauskas, D.A.; Krailo, M.D.; Meyers, P.A.; Schwartz, C.L.; Doski, J.; Gorlick, R.; Janeway, K.A.; Isakoff, M.S. Factors influencing survival after recurrence in osteosarcoma: A report from the Children's Oncology Group. *Pediatr. Blood Cancer* **2019**, *66*, e27444. [CrossRef]
13. Hashimi, M.; Hasan, O.; An, Q.; Miller, B.J. Novel scoring criteria for preoperative prediction of neoadjuvant chemotherapy response in osteosarcoma. *Iowa Orthop. J.* **2021**, *41*, 19.
14. Gianferante, D.M.; Mirabello, L.; Savage, S.A. Germline and somatic genetics of osteosarcoma—Connecting aetiology, biology and therapy. *Nat. Rev. Endocrinol.* **2017**, *13*, 480–491. [CrossRef]
15. Yu, D.; Zhang, S.; Feng, A.; Xu, D.; Zhu, Q.; Mao, Y.; Zhao, Y.; Lv, Y.; Han, C.; Liu, R. Methotrexate, doxorubicin, and cisplatinum regimen is still the preferred option for osteosarcoma chemotherapy: A meta-analysis and clinical observation. *Medicine* **2019**, *98*, e15582.
16. Bae, Y.H.; Park, K. Targeted drug delivery to tumors: Myths, reality and possibility. *J. Control. Release* **2011**, *153*, 198–205. [CrossRef]
17. Mouriño, V.; Boccaccini, A.R. Bone tissue engineering therapeutics: Controlled drug delivery in three-dimensional scaffolds. *J. R. Soc. Interface* **2010**, *7*, 209–227. [CrossRef]
18. Phull, S.S.; Yazdi, A.R.; Ghert, M.; Towler, M.R. Bone cement as a local chemotherapeutic drug delivery carrier in orthopedic oncology: A review. *J. Bone Oncol.* **2021**, *26*, 100345. [CrossRef]
19. Khan, S.A.; Akhtar, M.J. Structural modification and strategies for the enhanced doxorubicin drug delivery. *Bioorg. Chem.* **2022**, *120*, 105599. [CrossRef]
20. Zhou, H.; Liang, C.; Wei, Z.; Bai, Y.; Bhaduri, S.B.; Webster, T.J.; Bian, L.; Yang, L. Injectable biomaterials for translational medicine. *Mater. Today* **2019**, *28*, 81–97. [CrossRef]
21. Xia, X.; Shi, R.; Huang, J.; Li, Y.; Zuo, Y.; Li, J. Development of a phase change microcapsule to reduce the setting temperature of PMMA bone cement. *J. Appl. Biomater. Funct. Mater.* **2020**, *18*, 2280800020940279. [CrossRef]
22. Graça, M.P.F.; Gavinho, S.R. Calcium phosphate cements in tissue engineering. In *Contemporary Topics About Phosphorus in Biology and Materials*; IntechOpen: London, UK, 2020; p. 1.
23. Xu, H.H.; Wang, P.; Wang, L.; Bao, C.; Chen, Q.; Weir, M.D.; Chow, L.C.; Zhao, L.; Zhou, X.; Reynolds, M.A. Calcium phosphate cements for bone engineering and their biological properties. *Bone Res.* **2017**, *5*, 1–19. [CrossRef]
24. Saleh, A.T.; Raheem, A.A. Injectable Calcium Phosphate Cements (CPCs), Mechanical and Biological Properties, Applications in the Drug Delivery: A Review. *Int. Res. J. Mod. Eng. Technol. Sci.* **2021**, *3*, 887–895.
25. Otsuka, M.; Matsuda, Y.; Suwa, Y.; Fox, J.L.; Higuchi, W.I. A novel skeletal drug delivery system using a self-setting calcium phosphate cement. 5. Drug release behavior from a heterogeneous drug-loaded cement containing an anticancer drug. *J. Pharm. Sci.* **1994**, *83*, 1565–1568. [CrossRef]
26. Ginebra, M.-P.; Traykova, T.; Planell, J.A. Calcium phosphate cements: Competitive drug carriers for the musculoskeletal system? *Biomaterials* **2006**, *27*, 2171–2177. [CrossRef]
27. Singh, L.; Jain, H.; Sharma, P.; Singh, M.; Ezebuiro, V. Functionalized hydroxyapatite nanocomposites for localized drug delivery in bone cancer. *Hybrid. Adv.* **2026**, *12*, 100609. [CrossRef]
28. Liu, Y.; Nadeem, A.; Sebastian, S.; Olsson, M.A.; Wai, S.N.; Styring, E.; Engellau, J.; Isaksson, H.; Tägil, M.; Lidgren, L. Bone mineral: A trojan horse for bone cancers. Efficient mitochondria targeted delivery and tumor eradication with nano hydroxyapatite containing doxorubicin. *Mater. Today Bio* **2022**, *14*, 100227. [CrossRef]
29. Yoshikawa, H.; Myoui, A. Bone tissue engineering with porous hydroxyapatite ceramics. *J. Artif. Organs* **2005**, *8*, 131–136. [CrossRef]
30. Kandori, K.; Toshima, S.; Wakamura, M.; Fukusumi, M.; Morisada, Y. Effects of modification of calcium hydroxyapatites by trivalent metal ions on the protein adsorption behavior. *J. Phys. Chem. B* **2010**, *114*, 2399–2404. [CrossRef]
31. Hutchins, K.M. Functional materials based on molecules with hydrogen-bonding ability: Applications to drug co-crystals and polymer complexes. *R. Soc. Open Sci.* **2018**, *5*, 180564. [CrossRef]

32. Lindner, D.; Raghavan, D. Intra-tumoural extra-cellular pH: A useful parameter of response to chemotherapy in syngeneic tumour lines. *Br. J. Cancer* **2009**, *100*, 1287–1291. [CrossRef]
33. Abdelrahim, M.; Victor, D.; Esmail, A.; Kodali, S.; Graviss, E.A.; Nguyen, D.T.; Moore, L.W.; Saharia, A.; McMillan, R.; Fong, J.N. Transarterial chemoembolization (TACE) plus sorafenib compared to TACE alone in transplant recipients with hepatocellular carcinoma: An institution experience. *Cancers* **2022**, *14*, 650. [CrossRef]
34. Pavone-Macaluso, M.; Tripi, M.; Ingargiola, G.; Corselli, G.; Pavone, C.; Serretta, V. Current views on intravesical treatment and chemoprophylaxis of superficial bladder cancer. The present role of epirubicin and doxorubicin. *J. Chemother.* **1993**, *5*, 207–211. [CrossRef]
35. Kim, Y.; Brodt, M.D.; Tang, S.Y.; Silva, M.J. MicroCT for scanning and analysis of mouse bones. In *Skeletal Development and Repair: Methods and Protocols*; Humana Press: New York, NY, USA, 2021; pp. 169–198.
36. Almuhaideb, A.; Papathanasiou, N.; Bomanji, J. 18F-FDG PET/CT imaging in oncology. *Ann. Saudi Med.* **2011**, *31*, 3–13. [CrossRef]
37. Liu, Y.; Raina, D.B.; Sebastian, S.; Nagesh, H.; Isaksson, H.; Engellau, J.; Lidgren, L.; Tägil, M. Sustained and controlled delivery of doxorubicin from an in-situ setting biphasic hydroxyapatite carrier for local treatment of a highly proliferative human osteosarcoma. *Acta Biomater.* **2021**, *131*, 555–571. [CrossRef]
38. Liu, Y.; Corbascio, T.; Huang, J.; Engellau, J.; Lidgren, L.; Tägil, M.; Raina, D.B. Surgery Combined with Local Implantation of Doxorubicin-Functionalized Hydroxyapatite Halts Tumor Growth and Prevents Bone Destruction in an Aggressive Osteosarcoma. *J. Funct. Biomater.* **2024**, *15*, 232. [CrossRef]
39. Yang, Z.; Yu, S.; Li, D.; Gong, Y.; Zang, J.; Liu, J.; Chen, X. The effect of PLGA-based hydrogel scaffold for improving the drug maximum-tolerated dose for in situ osteosarcoma treatment. *Colloids Surf. B Biointerfaces* **2018**, *172*, 387–394. [CrossRef]
40. Aston, W.J.; Hope, D.E.; Nowak, A.K.; Robinson, B.W.; Lake, R.A.; Lesterhuis, W.J. A systematic investigation of the maximum tolerated dose of cytotoxic chemotherapy with and without supportive care in mice. *BMC Cancer* **2017**, *17*, 684. [CrossRef]
41. Zhang, K.; Zhou, Y.; Xiao, C.; Zhao, W.; Wu, H.; Tang, J.; Li, Z.; Yu, S.; Li, X.; Min, L. Application of hydroxyapatite nanoparticles in tumor-associated bone segmental defect. *Sci. Adv.* **2019**, *5*, eaax6946. [CrossRef]
42. Rodriguez-Galindo, C.; Shah, N.; McCarville, M.B.; Billups, C.A.; Neel, M.N.; Rao, B.N.; Daw, N.C. Outcome after local recurrence of osteosarcoma: The St. Jude Children's Research Hospital experience (1970–2000). *Cancer Interdiscip. Int. J. Am. Cancer Soc.* **2004**, *100*, 1928–1935.
43. Andreou, D.; Bielack, S.S.; Carrle, D.; Kevric, M.; Kotz, R.; Winkelmann, W.; Jundt, G.; Werner, M.; Fehlberg, S.; Kager, L.; et al. The influence of tumor- and treatment-related factors on the development of local recurrence in osteosarcoma after adequate surgery. An analysis of 1355 patients treated on neoadjuvant Cooperative Osteosarcoma Study Group protocols. *Ann. Oncol.* **2011**, *22*, 1228–1235. [CrossRef]
44. Mahvi, D.A.; Liu, R.; Grinstaff, M.W.; Colson, Y.L.; Raut, C.P. Local cancer recurrence: The realities, challenges, and opportunities for new therapies. *CA Cancer J. Clin.* **2018**, *68*, 488–505. [CrossRef]
45. Wang, Z.; Kregel, M.; Meijers, J.-L.; Franch, J.; Cuijpers, V.M.; Ahlers, D.; Karst, U.; Slootweg, P.; van der Geest, I.C.; Leeuwenburgh, S.C. Cisplatin-functionalized dual-functional bone substitute granules for bone defect treatment after bone tumor resection. *Acta Biomater.* **2025**, *191*, 158–176. [CrossRef]
46. Martine, L.C.; Holzapfel, B.M.; McGovern, J.A.; Wagner, F.; Quent, V.M.; Hesami, P.; Wunner, F.M.; Vaquette, C.; De-Juan-Pardo, E.M.; Brown, T.D. Engineering a humanized bone organ model in mice to study bone metastases. *Nat. Protoc.* **2017**, *12*, 639–663. [CrossRef]

Disclaimer/Publisher's Note: The statements, opinions and data contained in all publications are solely those of the individual author(s) and contributor(s) and not of MDPI and/or the editor(s). MDPI and/or the editor(s) disclaim responsibility for any injury to people or property resulting from any ideas, methods, instructions or products referred to in the content.